Title
THE ANGULAR DISTRIBUTION OF THE REACTION p + p-> d + n+

Author
Stevenson, M. Lynn.

Publication Date
1953-04-01

UCRL-2188

cy 3

UNIVERSITY OF CALIFORNIA — BERKELEY

RADIATION LABORATORY

DISCLAIMER

UCRL-2188

UNIVERSITY OF CALIFORNIA

Radiation Laboratory

Contract No. W-7405-eng-48

THE ANGULAR DISTRIBUTION OF THE REACTION $p + p \rightarrow d + \pi^+$ AT 338 MEV

M. Lynn Stevenson
(Thesis)

April, 1953

Berkeley, California

TABLE OF CONTENTS

THE ANGULAR DISTRIBUTION OF THE REACTION $p + p \rightarrow d + \pi^+$ AT 338 MEV

M. Lynn Stevenson

Radiation Laboratory, Department of Physics,
University of California, Berkeley, California

April, 1953

I. ABSTRACT

The angular distribution of the reaction $p + p \rightarrow \pi^+ + d$ has been measured with the meson and deuteron detected in coincidence. Measurements were made at 30° and 90° in the center of mass system for an incident proton energy of 338 Mev. Similar measurements were made at 30°, 60° and 90° for 332 Mev protons. The center of mass cross sections are tabulated below.

Proton Energy Mev	Meson Energy in the c.m. Mev	θ_{cm}	$\frac{d\sigma}{d\Omega} \times 10^{30}$ cm^2 ster^{-1}
338 ± 1	21.5	30°	35.7 (1±0.11)
		90°	9.98(1±0.17)
332 ± 3	19.0	30°	33.6 (1±0.076)
		60°	15.0 (1±0.11)
		90°	9.92(1±0.075)

The angular distribution of the 338 Mev data is:

$$0.29\ (1 \pm 0.29) + \cos^2\theta$$

The angular distribution of the 332 Mev data obtained by a least squares fit of the data is:

$$0.32\ (1 \pm 0.16) + \cos^2\theta$$

The average of these two angular distributions is:

$$0.32\ (1 \pm 0.14) + \cos^2\theta.$$

THE ANGULAR DISTRIBUTION OF THE REACTION $p + p \rightarrow d + \pi^+$ AT 338 MEV

M. Lynn Stevenson

Radiation Laboratory, Department of Physics,
University of California, Berkeley, California

April, 1953

II. INTRODUCTION

The early work on the positive meson production in proton proton collisions[1, 2] using nuclear emulsions showed in the center of mass system a predominant peak in the meson energy distribution at the maximum meson energy. This was of particular interest since, if there were no interaction of the final nucleons, the resulting spectrum should have shown no predominant peak.

Chew pointed out that if the interaction of the final nucleons were considered, one would obtain an energy spectrum with a peak at the upper energy end and a line spectrum corresponding to the formation of a deuteron by the neutron and proton.[3]

At this point, an attempt was made to detect the meson and deuteron in coincidence in order to add further evidence concerning the formation of the deuteron.[4]

The success of this preliminary experiment by electronic techniques initiated a program in which the angular distribution of the reaction $p + p \rightarrow \pi^+ + d$ was measured at 338 Mev, 332 Mev and 324 Mev.[5] In this program the meson and deuteron were detected in coincidence.

It is the purpose of this paper to report on this program with regard to the work at 338 Mev and 332 Mev.

III. EXPERIMENTAL METHOD

A. Preliminary Confirmation of Deuteron Formation

The experimental procedure used in the preliminary experiment which has been reported previously[4] will be reviewed briefly here.

1. Geometry

The essential features of the preliminary experiment can be seen in Fig. 1.

a. Target

The CH_2-carbon subtraction method was used employing a CH_2 target one inch in thickness.

b. Magnet

The magnetic field was used to analyze the momentum of the final products in the reaction and to separate these particles that came off in the forward direction from the main proton beam.

c. Counters

The detection equipment included two counter telescopes, each of which consisted of four counters containing the liquid scintillator terphenyl in xylene. These counters were 4 in. x 5 in. and were 3/4 in. thick. The two telescopes were placed in such a position that they would detect a meson deuteron event produced at about 10° in the center of mass system.

2. Electronics

Liquid scintillators were viewed by 1P21 and 1P28 photomultiplier tubes. The pulses from the photomultipliers were amplified with UCRL linear amplifiers, and were then passed through the variable gate units which formed square pulses of variable width and variable delay.

The linear amplifier pulses were mixed in a "tenth microsecond resolution" coincidence circuit. The output of this coincidence circuit and the variable gate pulses were mixed in "microsecond resolution" coincidence circuits. The outputs of these circuits were put into scaling circuits from which the data were recorded.

3. Particle Identification

a. Detection Efficiency

The use of the "slow" tenth microsecond equipment required that the deuteron counters be made insensitive to the high flux of diffraction-scattered protons that passed through the deuteron telescope. The counters were desensitized by decreasing the high voltage on the photomultipliers. Even though the deuteron pulse height was three times that of the diffraction-scattered proton pulse height, the amount by which the counters had to be desensitized was so great that the deuterons were detected with only 10 percent efficiency.

b. Momentum Measurement

As was mentioned earlier, the momentum of the particles was determined by the magnetic field combined with the measurement of the angular correlation of the particles.

c. Range Measurements

Range curves were obtained on both the meson and deuteron. The range and momentum then identified the mass of the particle.

The deuteron mass measured by this experiment was $2.2^{+0.6}_{-0.4}$ proton masses. The measured meson mass was 270^{+80}_{-90} electron masses. The errors correspond to the limits of uncertainty in the range and momentum measurements.

This preliminary experiment, while proving definitely the formation of the deuteron in the reaction $p + p \rightarrow d + \pi^+$, left much to be desired in the form of determining an absolute cross section.

The fact that the mesons passed through the fringe field of the magnet before they were detected meant that the solid angle subtended by the meson telescope was not known. The solid angle, of course, had to be known in an absolute cross section measurement. In addition, if an absolute measurement was to be made, the deuteron telescope could not be desensitized as much as it was.

These two factors required that the above experimental procedure be changed. The method by which the differential cross section at 30°, 60° and 90° in the center of mass system was measured at 338 Mev and 332 Mev will be the subject of the remainder of this paper.

B. Differential Cross Section Measurement

1. Geometry

A major change in the experimental method was made by discarding the magnetic field in order that the solid angle subtended by the meson counter would be known. Since the magnetic field was discarded, faster electronics were required and the amount of non-hydrogenous material in the beam had to be reduced.

a. Target Protons

The natural selection for the target was liquid hydrogen. The size of the target was determined by the allowable angular resolution and the size of available targets. This turned out to be a cylindrical target 1 gm/cm^2 thick of H_2 (5.6 inches in diameter). The essential features

of the system can be seen in Figure 2. The thin, wide aperture window was necessary because the mesons that are produced at large angles have very low energy.

b. Projectile Protons

Because of accidental coincidences between the meson counter and the deuteron counter, the "scattered" proton beam was used. The difference between the "scattered" beam and the electrically deflected beam is that the former beam lasts for about 20μ sec and the latter for only 0.2μ sec. This means that for the same average beam intensity the instantaneous beam intensity for the scattered beam is about 100 times as small as for the deflected beam. Since the accidental coincidence counting rate is proportional to the product of the instantaneous counting rates of the counters which are producing the coincidence, the scattered beam will produce orders of magnitude less accidental coincidences than will the deflected beam. Even though the scattered beam was used, the beam intensity had to be reduced by at least a factor of ten from the maximum available intensity.

The resolution of the coincidence circuit which was used was small compared to the fine structure of the beam. This fact was used to advantage in this experiment.

The nature of the time structure of the beam is as follows: Every 1/100th of a second the frequency of the cyclotron oscillator is modulated to bring the protons from the center of the cyclotron to the outer radius of the cyclotron. This is called the fm period. Approximately 300 equally spaced proton bursts occur within each fm period of the scattered beam. The individual separation is 6.0×10^{-8} sec. This period corresponds to the cyclotron resonant frequency when the protons are at the outer radius and is called the rf period. The duration of each of these pulses is of the order of $1/2 \times 10^{-8}$ sec which corresponds to the phase stable portion of each rf period. For the deflected beam, there are about three of these pulses per fm period. The physical configuration of the beam as it struck the target is shown in Figure 3. In order to eliminate scattering off the "48 inch collimator" walls, (see Figure 2a) the beam was pre-collimated at the pre-magnet collimator (see Figure 2b) and then brought down the center of the "48 inch collimator".

The beam was monitored with an ionization chamber of a known multiplication factor. The charge was collected on a condenser of known capacity. The number of protons that passed through the chamber was determined by the measured voltage that appeared across this condenser.

c. Orientation of Meson and Deuteron Counters

The angles that the meson and deuteron make with the incident proton beam for different center of mass angles can be seen most easily by making a non-relativistic velocity vector diagram of the constituents. This is shown in Figure 4. (This diagram, while giving approximate angles, makes large errors in the magnitude of the velocity vectors.)

The maximum laboratory angle can be seen to occur near 90° in the center of mass system. The angle in the laboratory system is approximately 6°. Hence, the deuterons will always be concentrated into a narrow cone, the vertex angle of which is about 6°.

This fact made it possible to place the deuteron counters at a sufficiently large distance from the target to make use of the difference in time-of-flight of the deuterons and the fast diffraction scattered protons in discriminating out a large fraction of these background protons (see Figure 5). As a typical example, a 2 in. x 2 in. meson counter was placed 24 in. from the target at such an angle as to correspond to 60° in the center of mass system. The 2 in. x 2 in. deuteron counter was placed at 144 inches from the target at the corresponding deuteron angle. If there had been no multiple coulomb scattering the deuteron counter would have counted all those deuterons which accompanied the mesons that entered the meson counter. The effect of multiple coulomb scattering of both meson and deuteron, combined with the finite size of the target, was that three out of four of these deuterons missed the deuteron counter.

The correct calculation of the dynamics of the reaction must of course be done relativistically. This is done in Appendix A.

The meson and deuteron laboratory angles corresponding to 30°, 60° and 90° in the center of mass system are summarized below for a proton energy of 338 Mev.

θ_{cm}	$\theta_{\pi\ lab}$	$\theta_{d\ lab}$
30°	15.5°	3.15°
60°	31.6°	5.22°
90°	49.2°	5.71°

d. Description of Counters

Liquid scintillators were used which contained 4 grams of terphenyl per 1000 grams of phenylcyclohexane. 38 milligrams of diphenylhexatriene was added to shift the spectrum to a more sensitive region of the photomultiplier.

As is shown in Figure 5, the meson telescope consisted of two counters; the first was 2 in. x 2 in. with a thickness of 1-1/2 inches (see Figure 6) and the second 3 in. x 3 in. x 1/2 in. A copper absorber was placed between these two counters so that the mesons could not penetrate into the rear counter.

The deuteron telescope also consisted of two counters. In the early experiments these were 2 in. x 2 in. x 1-1/2 in. and 3 in. x 3 in. x 3/4 in. for the front and rear counters, respectively. In the later experiments, these counters were increased in size to 3 in. x 3 in. x 5/8 in. and 4 in. x 4 in. x 5/8 in., respectively. (See Figure 7.) A copper absorber was placed between these two counters so that the deuterons could not penetrate into the rear counter.

Photographs of the meson and deuteron counter assemblies are shown in Figures 8a and 8b.

2. Electronics

The basic features of the particle detection scheme are shown in Figure 5. A more detailed sketch is shown in Figure 9. The light pulses from the liquid scintillator were converted into electrical pulses by means of RCA 5819 photomultipliers. These pulses were then amplified by Hewlett Packard type A (HPA) distributed amplifiers. The pulses from the first meson and deuteron counters after passing through three HPA's were mixed in a 6BN6 type coincidence circuit.[6] The time resolution of this coincidence circuit was of the order of 10^{-8} sec.

The 10^{-7} sec. output pulse from this coincidence circuit was amplified with a linear amplifier. This pulse then triggered a blocking oscillator which in turn triggered the sweep circuit of the E.G.G. Scope.

The pulses from the first meson and deuteron counters were put on the positive plate of the scope. This was done by passing the pulse from the output of the 2nd HPA through three HP type B distributed amplifiers. Suitable delay was placed in the meson and deuteron lines so that the two pulses would be separated on the scope by about 8×10^{-8} sec.

In a similar manner, the second meson and deuteron counter pulses were put on the negative plate of the scope. Again suitable delay was put in the lines so that the pulses appeared on the scope, equally spaced in 8×10^{-8} sec. intervals. The order of their appearance was M2 (negative), M1 (positive), D1 (positive), and D2 (negative).

The scope face was then photographed with a continuously moving 35 mm General Radio camera. The finished data were obtained by viewing the film with a Recordak projector.

Since neither meson nor deuteron could enter the rear counter in their respective telescopes, the meson deuteron event was characterized by two positive pulses as seen in Figure 10a.

Events that correspond to two high energy particles in accidental coincidence with each other are shown in Figure 10b. Figures 10c and 10d show accidental events in which one fast particle and one slow particle are involved in an accidental coincidence. Figure 10e shows a typical π-μ decay. The μ is seen on the trailing edge of the M1 pulse.

The film data gave all the information that was needed but, of course, it was not available until sometime after the experiment had been performed. Therefore, in order to know what was going on during the experiment, it was necessary to know the number of those traces which contained either one or both of the second meson or deuteron counter pulses.

This information was obtained by mixing the fast output of the M1D1 coincidence with the paralleled output of M2 and D2 third HPA amplifiers in a second 10^{-8} sec. 6BN6 coincidence circuit. The output of this coincidence circuit (called an "anti") was then mixed with the slow output of the M1D1 coincidence. This ensured that an "anti" count was not recorded when there was no recorded M1D1 count.

The output of this last coincidence circuit then gave the number of "anti" events. Hence, the difference between the total number of sweeps (M1D1 coincidences) and the number of "anti's" gave the number of events which involved two particles that did not enter the back counters of their respective telescopes.

It was not essential that this latter equipment be working perfectly, since the final data came from the film.

3. Particle Identification

a. Momentum Measurement

The momenta of the meson and deuteron were obtained by measuring the angles that these particles made with the proton beam centerline and by measuring the energy of the incident protons.

This can be easily illustrated by the following diagram:

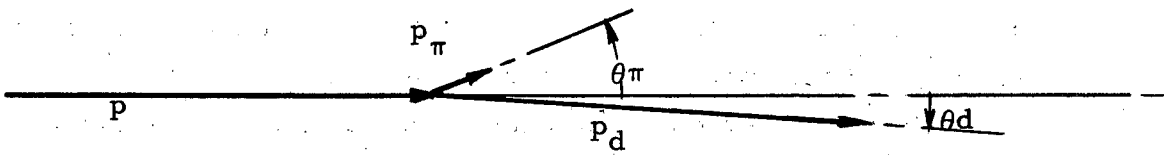

p = momentum of the incident proton beam.

p_π and p_d = momentum of the meson and deuteron, respectively.

$\theta\pi$ and θd = meson and deuteron angles, respectively.

$$p_\pi \sin \theta\pi - p_d \sin \theta d = 0 \qquad (\Sigma p_y = 0)$$

$$p_\pi \cos \theta\pi = p_d \cos \theta d = p \qquad (\Sigma p_x = p)$$

Solving for p_π and p_d

$$p_d = p \frac{\sin \theta\pi}{\sin (\theta\pi+\theta d)}$$

$$p_\pi = p \frac{\sin \theta d}{\sin (\theta\pi+\theta d)}$$

(1) Measurement of the Incident Proton Energy.

The technique used in measuring the beam energy was that used by Segrè and Mather[7]. This technique involved the measurement of the ratio of ionization produced in two ionization chambers. One measured the proton ionization after it had passed through a variable amount of copper. The other measured the ionization of the proton beam before it passed through the variable absorber.

Figure 11 is a plot of the observed ratio of ionization versus thickness of copper. The range, corresponding to 82 percent of the maximum ionization ratio, was 94.3 gms/cm^2 of copper. This value of the range, when refered to the range energy curves of Aron et al.,[8] gave the energy of the incident protons as 341 Mev.

(2) Measurement of the Meson and Deuteron Angles

The meson counter determined the angle and solid angle in the center of mass system.

The deuteron counter was moved in deuteron-counter width intervals to integrate all the deuterons that accompanied the mesons entering the meson counter. The deuteron integration curves, so obtained, are shown in Figure 12.

If the particles were assumed to be a meson and a deuteron, and the laboratory angles calculated to correspond to 90^o in the center of mass system, then the resulting deuteron angle is shown by the arrow in Figure 12. The meson counter was, of course, set at the above calculated meson angle.

From these measurements of the meson and deuteron angle plus the measurement of the incident proton momentum, the momenta of the two particles were determined.

b. Range Measurements

In order to determine the mass of the particles, the range must be known in addition to the momentum of the particles. Figure 13 shows typical range curves for the mesons and deuterons. Again the arrows represent the calculated mean range if the particles are assumed to be mesons and deuterons.

c. Auxiliary Measurements

(1) Velocity Measurement

(a) Time-of-Flight of the Deuteron

The fact that the deuteron counter could be placed a substantial distance from the target made it possible to obtain a velocity measurement of the deuteron to about 10 percent accuracy.

For the geometry as shown in Figure 5 the deuterons arrived at their counter approximately 3×10^{-8} sec. later than the mesons arrived at their counter. This, of course, meant that the pulses from the meson counter had to be delayed 3×10^{-8} sec. in order for them to be coincident with the deuteron pulse. A typical delay curve

is shown in Fig. 14.

(b) Specific Ionization

The pulse height distribution of the particles relative to the pulse height distribution of protons of known velocity can be obtained from the film data. (See Fig. 15). This measurement could give an independent value of the velocity. This information, however, was not necessary since the momentum and range measurements adequately identified the particles.

(2) Observation of π-μ Decay.

The measurements at 90^{o} in the center of mass system involved mesons of sufficiently low energy that they were stopped in the meson counter rather than in the copper absorber between the first and second counters.

It was possible to detect the scintillation of the recoil μ mesons in the π-μ decay with 20 percent efficiency. This agreed very well with the calculated efficiency of 21 percent. The π-μ decay could not be detected with full efficiency because the π meson-energy-loss pulse obscured the subsequent μ pulse for a duration of about 3×10^{-8} sec. A typical π-μ decay pulse is shown in Fig. 10e. This measurement was not necessary for the particle identification but offered further evidence that π mesons were being detected in the meson counter.

4. Detection Efficiency

a. Pulse Height

By plotting the pulse height distribution of the mesons and deuterons and by knowing the limiting pulse height which would produce a coincidence, it was determined that only 0.01 percent of the events were lost because of insufficient pulse height. Typical pulse height distributions are shown in Fig. 15. The gaussian curves drawn through the data have the same area and the same full width at half-maximum as the observed distribution.

The above pulse height distributions had full-widths at half-maximum of 41 percent and 18 percent for the mesons and the deuterons, respectively. As can be seen, these distributions were well above the cutoff pulse height of the coincidence circuit.

b. Time Phasing Plateau

Considerable care was exercised in making certain that the coincidence circuit resolving time was broad enough to accomodate any inherent time distribution which might have existed in the deuteron time-of-flight. The distribution which would result from the thickness of the target amounts to about 0.3×10^{-8} sec.

As can be seen in Figure 14 of the typical delay curve, there is a flat region of about 0.8×10^{-8} sec. On both sides of this region the yield drops to zero. This flat region indicates that when the meson delay was centered on the delay curve the coincidence circuit was operating at full efficiency.

An independent measurement that leads one to this same conclusion employs the fact that if the output of the coincidence circuit gets too small the scope will be slower in triggering the sweep. If this happens, there will occur a shift to the left in the location of the pulses on the scope. This is called "jitter".

This "jitter", of course, will occur if the pulse height of the meson and/or deuteron becomes too small, or, if the pulses of adequate magnitude are out of time phase. The absence of this "jitter" enabled an independent measurement to be made on the time phasing efficiency.

These two independent measurements verified the fact that the coincidence circuit resolution was broad enough to accomodate the inherent time distribution with full efficiency.

c. Range Distribution

The finite-sized target, in addition to the effective aperture of the counters, produced an energy distribution in both the mesons and the deuterons. The energy distribution, of course, produced a corresponding distribution in the range of the particles. This distribution was much larger than that produced by range straggling. By observing the range curves one could determine that the mesons and deuterons were detected with full efficiency.

It should be pointed out that the range measurements and the pulse height measurements were not independent. For example, if the mesons were being detected with an amount of absorber in place corresponding to the mean range of the mesons, then one half of the meson pulse heights would lie below the cutoff pulse height and one half of them above.

The latter mesons were, of course, the only ones being detected. When, initially, there was no absorber and as the absorber was increased, the pulse height was observed to increase to a point that corresponded to the particle stopping in the rear of the counter and then to decrease in pulse height until the cutoff pulse height was reached. At this point, of course, a large fraction of the meson-deuteron events were not being detected.

d. Accidental Coincidences

In addition to the fast background particles which included diffraction scattered protons and protons resulting from p-p scattering, there were also particles that did not produce counts in the rear counter of either meson or deuteron telescope and, therefore, behaved as a true meson or deuteron coincidence.

In order to determine the number of this type of event, the pulse from the meson telescope was delayed by exactly 6.0×10^{-8} sec. relative to the deuteron counter pulse. This length of time, as has been explained earlier, is the time interval between scattered proton beam pulses. In this way, the number of the background pulses feeding into each channel of the coincidence circuit remained the same. The only difference, of course, was that there were no real events amoung the resulting coincidences. This technique gave the number of accidental coincidences that were being detected along with the real events when the meson pulses were not delayed. The number of accidental events were usually about 20 percent of the real events.

Since the number of accidental double coincidences per unit number of incident protons is proportional to the beam intensity, the 6×10^{-8} sec. delay measurement had to be made at the same beam intensity as with no delay. In practice, it was not possible to do this precisely. Consequently, the accidental coincidences had to be normalized to the same beam intensity as with no delay. A typical calculation of this sort will be found in Appendix B.

e. Spacial Integration of the Deuterons

Previous mention has been made that, because of multiple scattering, approximately three out of four of the meson-deuteron events were lost. The question might be raised as to why the deuteron counter was not made larger. The answer to this question is twofold.

Firstly, at 30° in the center of mass system, the deuteron laboratory angle was about 3°. Consequently, the deuteron telescope was very close to the main proton beam. Even with a larger counter, it would have been necessary to move the counter one counter width in both horizontal and vertical directions to ensure that all the events were being detected at the central position. This procedure would have required that the deuteron counter be moved almost into the main proton beam at one position. This, of course, could not have been tolerated. Secondly, in the earlier experiments it was thought that the beam energy could be measured by measuring the meson and deuteron angles. The smaller the deuteron counter the better the angles could be measured, consequently, small counters were chosen. This measurement, however, was not sufficient to give the proton beam energy to the desired precision.

(1) Amount Missed in the Corners of the Integration Pattern

If a view of the deuteron integration pattern is taken in the direction of the deuteron trajectory, the following typical integration pattern is seen:

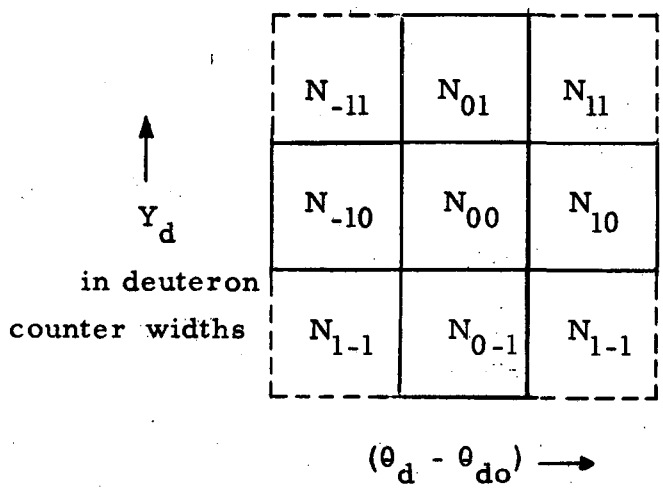

Typical Deuteron Integration Pattern

N_{ij} represents the number of counts obtained in the "i j th" cell. The cells enclosed by the solid lines represent areas in which actual measurements were made. A typical set of measurements can be seen in Fig. 12. Those cells which are partially enclosed by the dotted lines (i.e. the corners) represent areas for which the number of counts are calculated using adjacent measurements. For example:

$$N_{11} = \frac{N_{01}N_{10}}{N_{00}} \text{ and } N_{-11} = \frac{N_{-10}N_{01}}{N_{00}} \quad \text{etc.}$$

To obtain the total number of counts within the whole pattern, the counts in the individual cells are summed. In calculating the statistical error of this summed quantity one must remember that all the quantities involved are not statistically independent and should be treated accordingly.

For this particular type of integration pattern, a simple result is obtained.

$$N_{tot} = \frac{N_x N_y}{N_{00}} \left[1 \pm \left\{ \left[\frac{N_0}{N_x} + \frac{N_0}{N_y} - 1 \right]^2 \left(\frac{\delta N_{00}}{N_{00}} \right)^2 + \frac{\delta R_x^{\,2}}{N_x^2} + \frac{\delta R_y^{\,2}}{N_y^2} \right\}^{1/2} \right]$$

where $N_x \equiv \Sigma N_{i0}$ $\qquad R_x \equiv N_x - N_{00}$

$N_y \equiv \Sigma N_{0i}$ $\qquad R_y \equiv N_y - N_{00}$

The ratio of the detected events (i.e. $N_{00} + N_{10} + N_{-10} + N_{01} + N_{0-1}$ to N_{tot}) was of the order of 80 percent for most of the runs.

(2) Amount Outside the Integration Pattern

The foregoing calculations are concerned with finding the total number of counts which lie within the total integration pattern. In general, there will be events which lie outside this pattern.

The effect of multiple scattering is such as to produce a spacial distribution of deuterons which closely resembles a gaussian distribution. Each integration curve was essentially fit by a gaussian distribution. From this gaussian distribution of known half width, it was easy to calculate the fraction of the area under this gaussian that fell beyond the limit of the integration pattern. A gaussian was fitted to both the θ_d integration curve and the γ_d integration curve. The fraction missed in the θ_d integration plus the fraction missed in the γ_d integration gave the total fraction which was missed by the total integration pattern. This correction was usually about six percent.

f. Loss of Events by π-μ Decay in Flight

Since the mean life of the π^+ meson at rest is 2.6×10^{-8} sec, approximately 15 percent of the mesons decayed by the time they reached the meson counter. Of these mesons that decayed, a certain fraction could emit μ mesons in such a direction as to be detected by the meson counter. The result of a numerical integration which is described in Appendix D showed that about 50 percent of the mesons that decayed were counted as π-d events. This correction was the largest of all the corrections, with the exception of the amount in the corners of the integration pattern.

g. Loss of Events by Meson Nuclear Attenuation

The attenuation of the mesons in hydrogen and in stainless steel represented a small correction of the order of one percent. The total cross sections in hydrogen and copper, as measured by Stork[9], were used in calculating the meson attenuation.

h. Loss of Events by Deuteron Nuclear Attenuation

In addition to the attenuation in hydrogen and stainless steel, the deuterons were attenuated by the 12 feet of air and by the copper absorber which was placed in front of the deuteron telescope. The measured d-p cross section of Bloom[10] was used to calculate the attenuation in hydrogen. Measured deuteron cross sections[34] were used to calculate the attenuation in the stainless steel, the air and the copper. A typical set of corrections is tabulated below.

Attenuation in Percent	Attenuating Substance
2.5	H_2
0.2	8 mils Stainless Steel
0.9	12 ft. of air
2.5	Copper absorber

i. Loss of Coincidences by Electronic Dead Time

If the electronic equipment has a dead time during which time the circuit will not respond to two coincident pulses, the true counting rate will be given in the following expression:

$$N_{true} = \frac{n}{1 - n \tau d}$$

where n is the observed counting rate;

τ is the dead time of the coincidence circuit;

d is the duty factor of the beam.

τ_d was measured to be = 5.5 (1±.7) x 10^{-3} sec. and is in agreement with both the known dead time of 8 μ sec. and the approximate length of the scattered beam of 20 μ sec. The calculation using this value for τ_d gave a correction of less than one tenth percent for the measurements that involved the highest counting rates.

j. Other Corrections

(1) The Aperture of the Meson Counter

The finite size of the meson counter, in addition to the thickness of the target and multiple coulomb scattering, caused each measurement to be made over a finite angular interval in the center of mass system. The average value of the cross section over this interval is not, in general, equal to the value of the cross section at the center of this interval. Since the effective width of this interval in the center of mass system was known, a correction could be made. These corrections, for the angles measured, are tabulated below.

θ_{cm}	$\sigma_o/\bar{\sigma}_o$
30	1.004
60	1.000
90	0.983

σ_o is the value of the cross section at the center of the aperture, and $\bar{\sigma}_o$ is the average value of the cross section over the finite aperture.

(2) Deuteron Integration Angular Overlap

A further correction was made because the thick deuteron counter which was used in the early experiments overlapped a previously detected region in the integration pattern by a very slight amount. This can be seen in the following exaggerated figure.

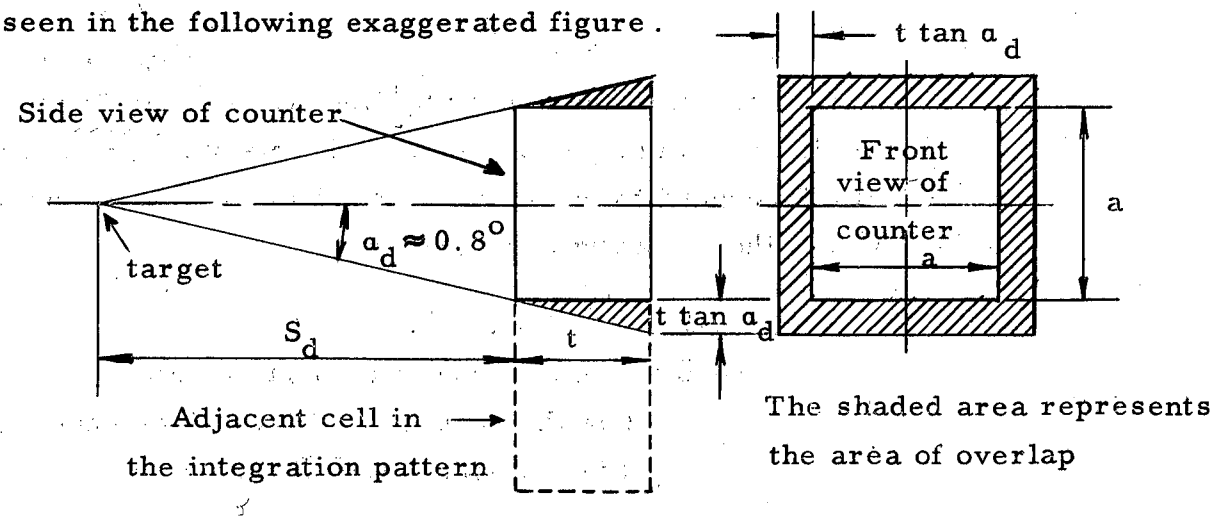

$$\text{Percent overlap} = \frac{4a \cdot t \cdot \sigma_d}{a^2} = \frac{2t}{S_d} \approx 2 \text{ percent}$$

When the spacial distribution of the deuterons was considered, this correction was reduced to about one percent.

(3) Effects of Scattering in the Walls of the Meson and Deuteron Counters

The multiple coulomb scattering and nuclear scattering in the walls of the scintillator increased the number of detected events over the number that would be detected if the walls were infinitely thin.

The following sketch demonstrates that both events (a) and (b) will be detectable, provided that both particles pass through a sufficient amount of scintillator. This means that the apertures of the counters are slightly larger than the apertures defined by the scintillator.

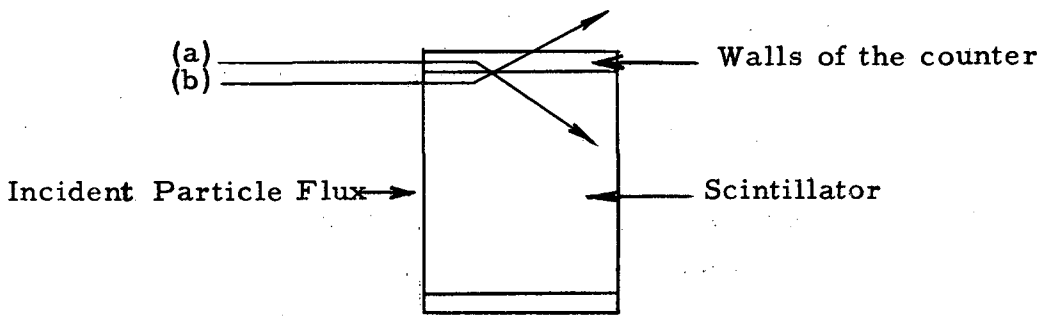

Side View of Counter

The net effect of this phenomenon in both the meson and the deuteron counters represents a four to five percent correction.

5. Discussion of Systematic Errors

For the purpose of estimating the overall r.m.s. error of the measured cross section, an error of 30 percent was assigned to each calculated systematic correction. In order to include these errors with the statistical error of the measurement the square of the errors were added. The combined error was given by the square root of this sum. In all cases, the overall r.m.s. error in the measurement was predominantely determined by the statistical error.

A measurement of the elastic p-p differential cross section at 90° in the center of mass system was made to reveal any unknown systematic error. The measured value was $3.3\ (1 \pm 0.1) \times 10^{-27}$ cm^2 ster^{-1}.

IV. SUMMARY AND ANALYSIS OF THE DATA

The data obtained for this experiment were collected over a period of seven months. The phase of the experiment being reported here can be divided into two parts; namely, the measurements at 338 Mev and the measurements at 332 Mev. This difference in energy was presumably caused by a change in the shape of a portion of the magnetic field at the outer radius of the cyclotron.

These data differ in one other respect; namely, the energy of the beam at 332 Mev is uncertain to plus or minus three or four Mev, whereas the beam energy at 338 Mev is known to plus or minus one Mev.

A. Summary of Differential Cross Section Measurements

The data which include all the corrections mentioned previously are summarized in Table I.

Measurements were made at 30°, 60° and 90° in the c.m. for the beam energy of 332 Mev; at 338 Mev only 30° and 90° c.m. measurements were made.

In most cases there are more than one measurement at each angle. To obtain the average value in such cases, each measurement was weighted inversely proportional to the square of their r.m.s. errors. The results of these averages are also listed in Table I.

TABLE I

Meson c.m. Energy	Proton Energy	θ_{lab}	$\theta_{c.m.}$	Date of Run	$\frac{d\sigma}{d\Omega} \times 10^{30}$ $\frac{cm^2}{ster}$		Averaged $\frac{\overline{d\sigma}}{d\Omega} \times 10^{30}$ $\frac{cm^2}{ster}$
					lab	c.m.	
19.0	332±3	15.13	29.6	10/17/52	119.5(1±0.097)	32.6 (1±0.10)	33.6 (1±0.076)
		15.6	30.5	11/19/52	129 (1±0.113)	35.2 (1±0.116)	
		30.97	59.5	8/9/52	51.0(1±0.15)	16.7 (1±0.15)	15.0 (1±0.11)
		30.93	59.5	10/15/52	42.2(1±0.15)	13.8 (1±0.15)	
		47.92	89.0	10/16/52	21.2(1±0.29)	9.65(1±0.29)	9.92 (1±0.075)
		47.92	89.0	10/17/52	24.7(1±0.22)	11.3 (1±0.22)	
		47.92	89.0	11/17/52	21.8(1±0.12)	9.92(1±0.12)	
		47.92	89.0	11/18/52	21.4(1±0.10)	9.75(1±0.11)	
21.5	338±1	15.4	29.6	1/7/53	126 (1±0.11)	35.7 (1±0.11)	35.7 (1±0.11)
		49.12	89.2	1/7/53	31.1(1±0.24)	14.9 (1±0.24)	9.98 (1±0.17)
		47.91	87.3	2/10/53	17.9(1±0.23)	8.55(1±0.23)	

B. Fitting of the Curve b $(a + \cos^2\theta)$ to the Data

Arguments are given in Section VI to show why only the second power of cos θ should appear in the angular distribution for the energies which are considered here.

The function b $(a + \cos^2\theta)$ was fitted to the 332 Mev data by the method of least squares. This method is described in Appendix C. The two data at 338, of course, determine a set of constants, a and b, without least squares fitting. The results of the two curve fittings are shown in Fig. 17. The large dots represent the average of the small dots. The following angular distributions for the 332 Mev and 338 Mev protons were obtained.

$$\frac{d\sigma}{d\Omega}_{332}(\theta) = 30 \left[0.32\ (1\pm0.16) + \cos^2\theta\right] \times 10^{-30}\ \text{cm}^2/\text{ster}$$

$$\frac{d\sigma}{d\Omega}_{338}(\theta) = 34 \left[0.29\ (1\pm0.29) + \cos^2\theta\right] \times 10^{-30}\ \text{cm}^2/\text{ster}$$

These curves are represented by the heavy lines in Fig. 17. To obtain the average of the two values of "a" each value of "a" was weighted by the inverse of the square of the respective r.m.s. errors. The average angular distribution between 332 Mev and 338 Mev is:

$$0.32\ (1\pm0.14) + \cos^2\theta.$$

V. COMPARISON OF DATA WITH OTHER MEASUREMENTS

A. $p + p \rightarrow \pi^+ + d$ Data of Cartwright et al., and V. Peterson at 340 Mev ($T_{\pi cm} = 22.5$)

The $p + p \rightarrow \pi^+ + d$ data of Cartwright, et al.[11] plus the data of V. Peterson[12] are shown in Fig. 18. These measurements were made at 340 Mev. The meson c.m. energy was 22.5 Mev. The solid curve represents the least squares fit of b $(a + \cos^2\theta)$ to these data, where b = 34 (1±0.18) and a = 0.11 (1±0.53).

B. $p + p \rightarrow \pi^+ + d$ Data of Crawford at 324 Mev ($T_{\pi cm} = 15.5$)

The angular distribution of $p + p \rightarrow \pi^+ + d$ at 324 was obtained by Crawford[5] who measured the absolute differential cross section at 90° c.m. This corresponds to a center of mass energy of 15.5 Mev. Crawford obtained the value of the 324 Mev cross section at 0° by using the

values of the 338 and 332 Mev cross sections at 0° as determined by the curve fitting discussed in this paper[5]. The excitation function measured by Schulz, et al.[13] was used to obtain the 0° cross section at 324 Mev. This analysis gave as the angular distribution;

$$23\ [0.28\ (1\pm0.25) + \cos^2\theta]\ \times 10^{-30}\ cm^2\ ster^{-1}$$

This curve is shown in Fig. 19.

C. $\pi^+ + d \rightarrow p + p$ Data of Durbin et al. for $T_{\pi cm} = 25$, 40 and 53 Mev.

The principle of detail balancing enables one to make a further comparison. This principle ensures that the forward and the inverse processes have the same angular dependence.

The measurements of Durbin, Loar and Steinberger[14] on the inverse reaction $\pi^+ + d \rightarrow p + p$ have been made for meson center of mass energies of 25 Mev, 40 Mev and 53 Mev.

These data are shown in Figs. 20a, 20b and 20c. The solid curves represent the least squares fits to the data. The results of the least squares fits are tabulated below:

Meson c.m. Energy	Angular Distribution
25	$9.7\ [(0.19\pm0.09) + \cos^2\theta] \times 10^{-28}$
40	$16\ [(0.26\pm0.14) + \cos^2\theta] \times 10^{-28}$
53	$18\ [(0.18\pm0.15) + \cos^2\theta] \times 10^{-28}$

D. $\pi^+ + d \rightarrow p + p$ Data of Clark et al. for $T_{\pi cm} = 23$ Mev

Measurements have also been made by Clark, Roberts and Wilson[15] on the inverse reaction. The geometry of this experiment was such that the detectors subtended a large interval in θ. The measured total cross section depended on the value of "a" which was assumed. The value of the total cross section was so insensitive to the value of "a" that, even if the true total cross section were known, "a" could not be determined with significant accuracy.

E. $n + p \rightarrow \pi^o + d$ Data of Hildebrand at 400 Mev ($T_{\pi cm} = 53$ Mev)

One of the most striking pieces of evidence in support of the hypothesis of charge independence of nuclear forces has been given by Hildebrand[16] with his measurement of the angular distribution of the reaction $n + p \rightarrow \pi^o + d$. This reaction was studied with 400 Mev

neutrons. This neutron energy corresponds to a meson c.m. energy of 53 Mev. The results of this experiment are shown in Fig. 21.

In the forward and inverse reactions, $p + p \rightleftarrows \pi^+ + d$, the angular distributions must necessarily be symmetrical about 90° c.m. because of the two identical particles in the initial or final state, respectively.

This condition however does not hold for the reaction $n + p \rightarrow \pi^0 + d$, since, in this case, it is possible to distinguish the 0° axis in the c.m. from the 180° axis. The 0° axis is the direction of the neutron and the 180° axis is the direction of the proton.

It has been shown by various authors[17,18,19] that the ratio of the cross section of $p + p \rightarrow \pi^+ + d$ to the cross section of $n + p \rightarrow \pi^0 + d$ should be 2, provided that there is charge independence of nuclear forces. This means that the angular distributions should be identical and, therefore, would require that the $n + p \rightarrow \pi^0 + d$ angular distribution be symmetrical about 90° in the center of mass system.

Not only is the experimental curve symmetric about 90° c.m., but the angular distribution is the same as the angular distribution of the reaction $\pi^+ + d \rightarrow p + p$ at 53 Mev, as shown in Fig. 20c.

F. Summary of the Angular Distributions

For the purpose of summarizing all the existing measurements that pertain to the angular distribution of $p + p \rightarrow \pi^+ + d$, the values of "a" versus the center of mass meson energy are plotted in Fig. 22. The value of "a" for $n + p \rightarrow \pi^0 + d$ is included for comparison.

A discussion of the energy variation of $a + \cos^2\theta$ will be given in the following section.

VI. COMPARISON OF DATA WITH THEORY

The fact that the π meson is a pseudo-scalar[20,21,22] allows one to make some general remarks about the contributing initial and final states in the reaction $p + p \rightarrow \pi^+ + d$.

The following diagram summarizes the requirements of conservation of angular momentum and parity. On the left side of the diagram, the allowable states for the p-p system are written. The subscripts denote

the total angular momentum of the states. The plus and minus signs refer to the parity of that state; the states of even orbital angular momentum being positive, the states of odd angular momentum being negative.

On the right side of the diagram the states of orbital angular momentum of the meson with respect to the center of mass of the π-d system are written. Again, the subscript refers to the total angular momentum, and the plus or minus sign to the parity of the system. The deuteron is a mixture of S and D states with total angular momentum of one. Therefore, since the meson is a pseudo-scalar (odd parity), the states of odd meson orbital angular momentum have even parity (+).

The solid lines connect states which have the same total angular momentum and parity and, therefore, represent allowed transitions.

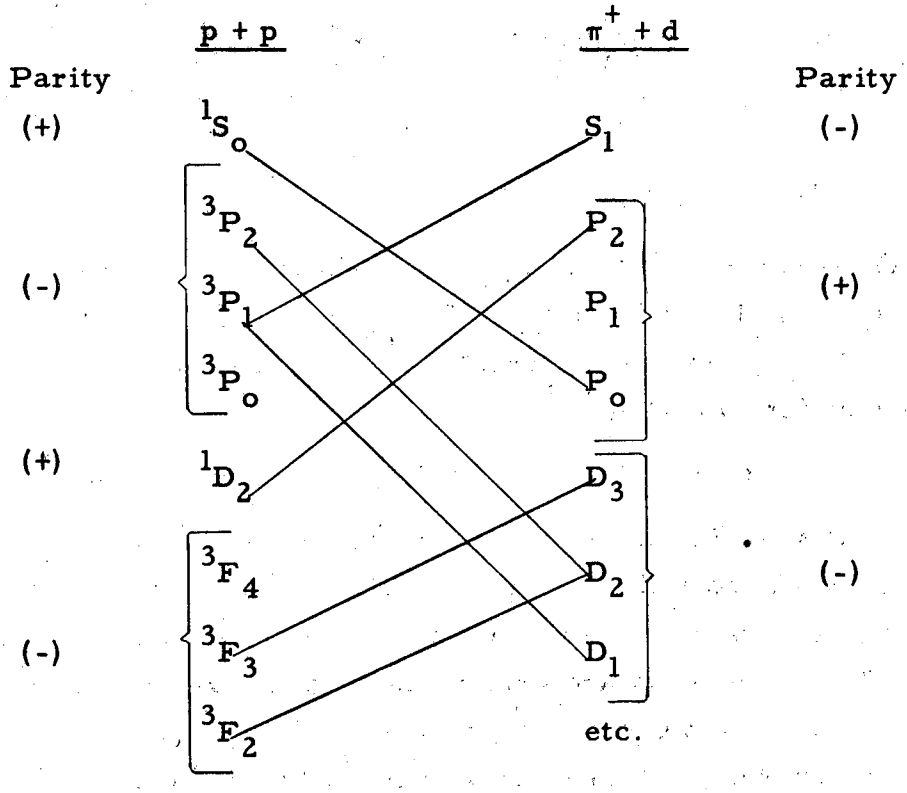

Since the meson energy in the center of mass system is only 20 Mev, the higher meson angular momentum states should not be expected to contribute appreciably; unless, however, there exist interactions which favor these states. There are no known interactions which

would favor D state over S and P state mesons. There is, however, strong evidence that P state mesons are favored over S state mesons even at 20 Mev.[18, 23] This leads to a great simplification of the problem, since all the meson D states can be neglected.

Just above meson production threshold S state mesons should be predominant in spite of the favored P state interaction. Rather than neglect this state entirely; the meson S state transition will be represented by a broken line in the following diagram.

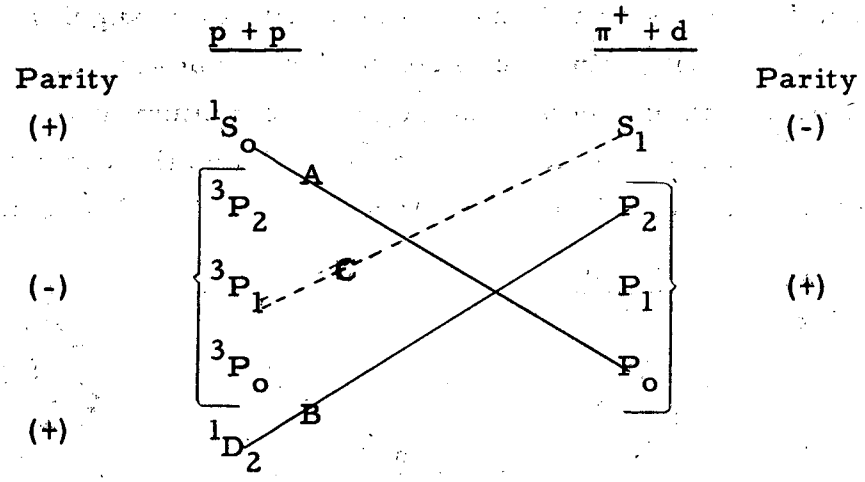

A and B represent the complex probability amplitudes for the transitions $(^1S_o)_{pp} \rightarrow (P_o)_{\pi d}$ and $(^1D_2)_{pp} \rightarrow (P_2)_{\pi d}$, respectively.

If only the A and B transitions are considered, the following angular distribution is obtained:[24, 25]

$$\sigma(\theta) \propto |A|^2 + \frac{3}{2} |B|^2 \left(\frac{1}{3} + \cos^2\theta\right) + 3\sqrt{2}\, R A^* B \left(\frac{1}{3} - \cos^2\theta\right)$$

It should be noted that if there were any S wave meson contribution ("C") it could contribute only a positive constant term to the above expression (i.e., there could be no interference). The reason for this is simple. The P wave mesons are produced by initial proton singlet states; whereas, the S wave mesons are produced by an initial proton triplet state. It is well known that there can be no interference between singlet and triplet states; therefore, the squares of the individual amplitudes are added to give the angular distribution.

It is interesting to note that:

a. If A = 0, then $\sigma(\theta) \propto 1/3 + \cos^2\theta$. This angular distribution could also be obtained by the following choice of A and B.

$$|A| = -\cos \alpha_{ab} \cdot 2\sqrt{2}\ |B|$$

where $A = |A|\ e^{i\alpha_a}$

$B = |B|\ e^{i\alpha_b}$

$\alpha_{ab} = \alpha_a - \alpha_b$

b. If B = 0, then $\sigma(\theta)$ is spherically symmetrical. This angular distribution could also be obtained by the following choice of A and B.

$$|B| = 2\sqrt{2}\ |A| \cos \alpha_{ab}$$

c. If the angular distribution were pure $\cos^2\theta$, then the only unique relation between A and B is obtained, namely:

$$A = -\frac{1}{\sqrt{2}}\ B$$

The examples a, b, and c illustrate the fact that the observed angular distributions can make no unique determination of A and B.

Chew et al.[25] have analysed this problem in terms of the weak coupling theory. The interaction was of the form $\vec{\sigma}_i \cdot [a \vec{\nabla}_n + b \vec{q}]\tau_i^+$ where the term $a \vec{\sigma} \cdot \vec{\nabla}_n$ involves the nucleon recoil and is responsible for the transition $(^3P_1)_{pp} \xrightarrow{C} (S_1)_{\pi d}$. The term $b \vec{\sigma} \cdot \vec{q}$ involves the meson momentum and produces the transitions $(^1S_o)_{pp} \xrightarrow{A} (P_o)_{\pi d}$, $(^1D_2)_{pp} \xrightarrow{B} (P_2)_{\pi d}$.

It can be seen that the weak coupling theory gives very different energy dependence for the S state and the P state.

The fact that the angular distribution is not changing rapidly with energy and is not spherically summetric indicates that, at the meson energies being considered, the $b \vec{\sigma} \cdot \vec{q}$ term is the important one. On the basis of this evidence plus the earlier evidence for predominant P state emission,[18, 23] the $a \vec{\sigma} \cdot \vec{\nabla}_n$ term was neglected.

The values of A and B evaluated in this way are:

$$A = F_o e^{i\delta o}$$

$$B = F_2 e^{i\delta 2}$$

where $F_o = \int_o^\infty u_f(r)\ u_i(r)\ dr$

$F_2 = \int_o^\infty w_f(r)\ w_i(r)\ dr$

u_i and w_i are the radial parts of the deuteron S and D wave functions[26], respectively, as defined by Rarita and Schwinger[26]. u_f and w_f are the diproton continuum S and D wave functions, respectively, normalized to $\sin(kr + \delta_0)$ and $\sin(kr + \delta_2 - \pi)$ at $r \to \infty$.

The quantity F_0/F_2 can be written in terms of the Fourier transforms[27] of the triplet NP central force $\equiv {}^3$(NP) central; the triplet NP tensor force $\equiv {}^3$(NP) tensor; and the singlet PP central force $\equiv {}^1$(PP).

$$\frac{F_o}{F_2} = \frac{3}{2\sqrt{2}} \left[\frac{{}^3\text{(NP) central} - {}^1\text{(PP)}}{{}^3\text{(NP) tensor}} \right]$$

The work of Pease and Feshbach[28] indicates that the ^{3}(NP) central force is equal to the ^{1}(PP) force. This means that F_o/F_2 or $|A|/|B|$ is zero. This, as was shown earlier, would give an angular distribution of $1/3 + \cos^2\theta$. Chew[29] pointed out that the central force part of the Levy potential[30] is the same in both singlet and triplet states and, therefore, would make $|A|/|B| = 0$.

By assuming a pure tensor force and by using pseudo-scalar meson theory with pseudo vector coupling, Foldy[31] obtained an angular distribution of $1/3 + \cos^2\theta$. When tensor forces were neglected, a spherically symmetric angular distribution was obtained.

Recent work of Brueckner and Watson[23, 32] has shown that the strong $j = 3/2$, $T = 3/2$ meson nucleon interaction that is indicated in the meson scattering experiments and in the photo meson production experiments would give an angular distribution in agreement with the present experiment. The reason is that the $j = 3/2$ meson nucleon interaction takes place in the $({}^1D_2)_{pp} \longrightarrow (P_2)_{\pi d}$ transition whereas the $j = 1/2$ interaction takes place in the $({}^1S_o)_{pp} \longrightarrow (P_o)_{\pi d}$ transition. If the $j = 3/2$ interaction predominates over the $j = 1/2$ interaction, B is much larger than A and an angular distribution of approximately $1/3 + \cos^2\theta$ is obtained.

As was mentioned previously, the presence of any S state meson production would contribute a positive constant term to the angular distribution. For this reason, the angular distribution is expected to become more spherically symmetric as the meson production threshold is approached.

Thus far, the measurements of the angular distribution at the lower energies have not shown any marked increase of "a". The data, however, are rather poor; as can be seen in Fig. 22. The aim of future experiments will be to ascertain, by means of the angular distribution, at what energies the S wave emission becomes more important than the P wave emission.

APPENDIX A

DYNAMICS OF $p + p \rightarrow \pi^+ + d$

E_0 = rest energy of the proton = 938.17 Mev.

E_{0d} = rest energy of the deuteron = 1875.41 Mev.

$E_{0\pi}$ = rest energy of the meson = 139.70 Mev.*

T = kinetic energy of the proton beam

E = total relativistic energy of a particle

E_t = total relativistic energy of the entire system

$c\bar{\beta}$ = velocity of the center of mass system

Primed quantities refer to values in the center of mass system.

$$(1) \qquad \bar{\beta} = \frac{\Sigma \vec{cpi}}{\Sigma Ei} = \sqrt{\frac{E - E_0}{E + E_0}} = \sqrt{\frac{T}{T + 2E_0}}$$

$$(2) \qquad \bar{\gamma} = (1 - \bar{\beta}^2)^{-1/2} = \sqrt{\frac{E + E_0}{2E_0}} = \sqrt{\frac{E_t}{2E_0}}$$

The energy of the entire system can be Lorentz-transformed into the center of mass system as a four-vector. This transformation gives a rather simple expression since the momentum of the entire system is zero in the center of mass.

$$(3) \qquad E_t = \bar{\gamma} \left[(\bar{\beta} cp_t = 0) + E_t' \right]$$

$$E_t' = \left(\frac{1}{\bar{\gamma}} = \sqrt{\frac{2E_0}{E_t}} \right) E_t$$

$$E_t' = \sqrt{2E_t E_0}$$

This gives the available relativistic energy in the c.m. to be shared by the meson and deuteron.

$$(4) \qquad E_t' \overset{\text{Energy conservation}}{\downarrow} = E_\pi' + E_d' = E_\pi' + \sqrt{(cp_d' = \sqrt{E_\pi'^2 - E_0^2})^2 + E_{0d}^2}$$

$\uparrow$ Momentum conservation

---

* The value of the π^+ meson mass used in these calculations was 273.5 e.m. It was assumed that the π^+ mass was the same as the π^- mass as measured by Crowe.[33]

$$(5)\quad E_\pi' = \frac{E_t'^2 - E_{0d}^2 + E_{0\pi}^2}{2E_t'} = \gamma'_\pi E_{0\pi}, \qquad \gamma'_\pi = (1 - \beta'^2_\pi)^{-1/2}$$

$$(6)\quad E_d' = E_t' - E_\pi' = \gamma'_d E_{0d}, \qquad \gamma'_d = (1 - \beta'^2_d)^{-1/2}$$

$$(7)\quad cp_\pi' = \sqrt{E_\pi'^2 - E_{0\pi}^2} = cp_d'$$

The meson and deuteron energies in the center of mass system are then Lorentz-transformed back into the laboratory system. A convenient parameter with which to express the laboratory quantities is the meson center of mass angle.

$$(8)\quad E_\pi = \bar{\gamma}(\bar{\beta}\, cp_\pi' \cos\theta' + E_\pi') = T_\pi + E_{0\pi}$$

$$E_d = E_t - E_\pi$$

The relation between center of mass angles and laboratory angles is expressed as follows.

$$(9)\quad \tan\theta = \frac{\sin\theta'}{\bar{\gamma}\left(\frac{\bar{\beta}}{\beta'} + \cos\theta'\right)}$$

where $c\beta'$ is the velocity of a particle in the c.m.

The transformation of the laboratory solid angle ($d\phi d(\cos\theta) \equiv d\Omega$) to the center of mass solid angle ($d\phi d(\cos\theta') \equiv d\Omega'$) is given by the following:

$$(10)\quad \frac{d\Omega'}{d\Omega}(\theta) = \frac{\bar{\gamma}^2}{\left(1 + \frac{\bar{\beta}}{\beta'}\cos\theta'\right)} \left(\frac{\frac{\bar{\beta}}{\beta'} + \cos\theta'}{\cos\theta}\right)^3$$

where θ is determined by eq. (9)

This factor was used to obtain the center of mass differential cross section from the laboratory differential cross section.

APPENDIX B

SAMPLE CALCULATION

To illustrate the manner in which the data were reduced, a typical run will be considered. For each run the number of integrator volts (I), the time duration of the run (Δt) and the number of meson-deuteron pulses (M1D1) (see Figs. 10a and 10e) were tabulated.

Runs were made in pairs, one run being made with no delay in the meson counter and the other with 6.0×10^{-8} sec. delay. The latter run determined, within the statistical error, the number of accidental M1D1 pulses which occured during the run with no delay.

90° c.m. 1-7-53 338 Mev

Run	I	Δt min	$\frac{dI}{dt} = \dot{I}$	M1D1	$\left(\frac{\overset{y}{\overset{\shortparallel}{M1D1}}}{I}\right)$ $\left(\pm\delta y^2\right)$	$\overset{N}{\overset{\shortparallel}{y(0)-(y(6))}}$	Meson Delay
147	1.266	6.12	0.207	56	44.2 34.9		0×10^{-8} sec.
					(4.9) (8.0)	39.3±6.6	
148	0.712	4.00	0.178	3	4.2 5.9		6.0×10^{-8} sec.

The number of accidental M1D1 events per integrator volt is proportional to the beam intensity. This is shown below:

$$\frac{d\,(M1D1)}{dt} \propto \frac{dn_{M1}}{dt} \cdot \frac{dn_{D1}}{dt} = \left(\frac{dI}{dt}\right)^2 \cdot \frac{dn_{M1}}{dI} \cdot \frac{dn_{D1}}{dI}$$

but dn_{M1}/dI and dn_{D1}/dI are constants, therefore:

$$\frac{d(M1D1)}{dI} \propto \frac{dI}{dt}$$

The value enclosed by parenthesis in the above table represents the accidentals, y(6), normalized to the same beam intensity as the zero delay beam intensity.

$$(y(6)) = \frac{\dot{I}(0)}{\dot{I}(6)} \quad y\,(6).$$

This value is then subtracted from y(0) to obtain the true number of meson-deuteron events per integrator volt $\equiv$ N.

There were usually several such numbers obtained at the same position in the integration pattern. In order to obtain the average value of these data, each measurement was weighted by the inverse square of their respective r.m.s. errors.

$$\bar{N} = \frac{\Sigma \frac{1}{\delta N_i^2} \cdot N_i}{\Sigma \frac{1}{\delta N_i^2}} \pm \frac{1}{\sqrt{\Sigma \frac{1}{\delta N_i^2}}}$$

A typical example is tabulated below

N_i	$(\delta N_i)^2$	$10^2/(\delta N_1)^2$	$(10^2/\delta N_1^2)\ N_i$
31.8	23.6	4.23	135.0
39.1	43.7	2.29	89.5
29.9	33.6	2.98	89.0
23.9	72.3	1.38	33.1
		Σ=10.88	Σ=346.6
	$\bar{N} = 31.8 \pm 3.0$		

The procedure that was used in obtaining the total number of meson-deuteron events within the entire integration pattern was discussed in the section under Detection Efficiency.

For the particular case that was presented in that section, a simple relation was obtained:

$$N_t = \frac{N_x N_y}{N_{00}} \left| 1 \pm \left\{ \left[\frac{N_0}{N_x} + \frac{N_0}{N_y} - 1 \right]^2 \left(\frac{\delta N_{00}}{N_{00}} \right)^2 + \frac{\delta R_x^2}{N_x^2} + \frac{\delta R_y^2}{N_y^2} \right\}^{1/2} \right|$$

A typical calculation is presented below.

$$N_{00} = 31.8 \pm 3.03$$

$N_{10} = 5.7 \pm 4.1$ $\qquad$ $N_{01} = 17.2 \pm 6.2$

$N_{-10} = 1.7 \pm 6.2$ $\qquad$ $N_{0-1} = 2.2 \pm 5.5$

$N_x = N_{00} + N_{10} + N_{-10}$ $\qquad$ $N_y = N_{00} + N_{01} + N_{0-1}$

$N_x = 39.2$ $\qquad$ $N_y = 51.2$

$$N_t = \frac{N_x N_y}{N_{00}} = 63.1$$

$$\frac{N_0}{N_x} = 0.812 \qquad \frac{N_0}{N_y} = 0.612 \qquad \frac{\delta N_0}{N_0} = 9.53 \times 10^{-2}$$

$$R_x^2 = 54.0 \qquad R_y^2 = 44.0$$

$$\frac{\delta N_t}{N_t} = 0.23$$

The various corrections to be made to N_t were also discussed in the section under Detection Efficiency. A typical set of corrections is tabulated below.

Correction in Percent	Type of Correction
+ 1.3	Number falling outside the integration pattern
+ 5.0	π-μ decay in flight
- 0.7	Scattering by the deuteron counter walls
- 1.3	Overlap of deuteron integration pattern
- 4.8	Scattering by the meson counter walls
+ 6.1	Deuteron loss by nuclear attenuation
+ 0.3	Meson loss by nuclear attenuation
- 1.7	Correction for the finite aperture of the meson counter.

The corrected value of N_t is $1.042 \times 63.1\ (1\pm0.23) = 65.7\ (1\pm0.23)$.

The laboratory cross section is obtained from this corrected value of N_t by knowing: (a) the solid angle subtended by the meson counter ($\Delta\Omega_{lab}$), (b) the number of incident protons per integrator volt (N_{inc}) and (c) the number of target protons per cm^2 (N target).

$$\frac{d\sigma}{d\Omega}_{lab} = N_t / \left(N_{inc}\, N_{target}\, \Delta\Omega_{lab}\right)$$

For the example that has been considered thus far:

$N_{inc} = 7.79 \times 10^8$ protons/integrator volt
$N_{target} = 6.02 \times 10^{23}$ protons/cm^2
$\Delta\Omega_{lab} = 4.56 \times 10^{-3}$ ster.

The resulting laboratory cross section is:

$$\frac{d\sigma}{d\Omega}_{lab} (90^{\circ} \text{ c.m.}) = 31.1\ (1 \pm 0.23) \times 10^{-30} \text{ cm}^2/\text{ster}$$

The center of mass cross section is obtained by multiplying

$$\frac{d\sigma}{d\Omega}_{lab} (90^{\circ} \text{c.m.}) \quad \text{by} \left(\frac{d\Omega}{d\Omega'} (90^{\circ} \text{ c.m.}) = 0.479\right).$$

$$\frac{d\sigma}{d\Omega}_{c.m.} (90^{\circ} \text{ c.m.}) = 14.9\ (1 \pm 0.23) \times 10^{-30} \text{ cm}^2/\text{ster}.$$

APPENDIX C

METHOD OF LEAST SQUARES

The curve to be fit to the data is

$$y(x) = a_0 + a_1 \quad (x \equiv \cos^2\theta)$$

where: $y_i \pm \delta y_i$ is the i th measurement at the point x_i.

$\frac{1}{\delta y_i^2} = p_i$ is the weight of the i th measurement.

$$D = \begin{vmatrix} \Sigma p_i & \Sigma p_i x_i \\ \Sigma p_i x_i & \Sigma p_i x_i^2 \end{vmatrix}$$

$$Da_0 = \begin{vmatrix} \Sigma p_i y_i & \Sigma p_i x_i \\ \Sigma p_i x_i y_i & \Sigma p_i x_i^2 \end{vmatrix}$$

$$Da_1 = \begin{vmatrix} \Sigma p_i & \Sigma p_i y_i \\ \Sigma p_i x_i & \Sigma p_i x_i y_i \end{vmatrix}$$

The summation is made over all the measured points to which the curve is being fit.

The errors of the constants a_0 and a_1 are given by:

$$D\delta a_0^2 = A_{00} = \Sigma p_i x_i^2$$

$$D\delta a_1^2 = A_{11} = \Sigma p_i \qquad A_{ij} \text{ is the ij th cofactor of D}$$

$$D\delta a_0 \delta a_1 = A_{01} = -\Sigma p_i x_i$$

The value of "a" in $a + \cos^2\theta$ together with the r. m. s. error is then obtained as follows:

$$a = \frac{a_0}{a_1}\left\{1 \pm \left[\left(\frac{\delta a_0}{a_0}\right)^2 + \left(\frac{\delta a_1}{a_1}\right)^2 - \frac{\overline{2\delta a_0 \delta a_1}}{a_0 a_1}\right]^{1/2}\right\}$$

APPENDIX D

π-μ DECAY IN FLIGHT CORRECTION

(1) $d^2N(\theta,\phi)$ is the number of π mesons produced within the solid angle $\sin\theta\, d\theta\, d\phi$. $d^2N(\theta,\phi) = k \cdot d\sigma/d\Omega_{lab}(\theta) \sin\theta\, d\theta\, d\phi$.

(2) $f(r,\theta,\phi)\, dr$ is the fraction of this number that decay in the interval r to r + dr.

$$f(r,\theta,\phi)\, dr = e^{-ar}\, d(ar)$$

where $a = \dfrac{1}{c\tau_0\beta\gamma}$

$c\beta$ = velocity of the π meson

$\gamma = (1-\beta^2)^{-1/2}$

τ_0 = mean life of the π meson at rest.

(3) $\Delta\Omega'(r, \theta\, \phi)/4\pi$ is the probability that the μ meson in the π-μ decay will enter the meson counter. $\Delta\Omega'$ is the solid angle subtended by the meson counter in the π meson rest frame.

(4) $g(\theta,\phi)$ is a function which is unity if the π meson velocity vector lies within the solid angle subtended by the meson counter, and is zero if it lies outside.

(5) $$\int_\theta \int_\phi \int_r d^2N(\theta,\phi)\, f(r,\theta,\phi)\, \frac{\Delta\Omega'(r,\theta,\phi)}{4\pi}\, dr \equiv A$$

This is the total number of π-μ decays which are counted as π-d events. In other words, the decay μ entered the first meson counter but did not enter the second, and was in coincidence with a deuteron.

(6) $$\int_\theta \int_\phi d^2N(\theta,\phi)\, g(\theta,\phi)\, e^{-\hat{a}s} \equiv B.$$

This is the number of counted π-d events in which the π meson did not decay. s is the distance from the meson counter to the target.

(7) $$\int_\theta \int_\phi d^2N(\theta,\phi)\, g(\theta,\phi) \equiv C$$

This is the number of counted π-d events there would be if the mean life of the π meson were infinite.

The correction factor that must be applied to the data is the ratio of counted events that there would have been if the π mean life had been infinite to the number of counted events there would have been with a meson mean life of τ_0. This factor is $C/(A + B)$.

The factor $A/(C - B)$ was determined by numerical integration. The μ mesons, when emitted in the direction of the π meson velocity, had sufficient energy to penetrate the rear meson counter. This event would not have been recorded as a π-d event. This phenomenon plus the determination of $\Delta\Omega'$ made the integration very tedious.

A calculation combining numerical integration and the Monte Carlo method is being made to check the numerical integration of $A/(C - B)$.

The dynamics of the π-μ decay which is necessary for these calculations will be published in another report. (UCRL 3481)

ACKNOWLEDGMENTS

I wish to express my appreciation to Dr. Herbert F. York Jr. for his valuable suggestions concerning the experimental techniques and to Dr. Frank S. Crawford Jr. for his collaboration on the experiment. I am particularly indebted to Professor Luis Alvarez for his interest in the experiment and for his personal kindness. I am grateful to Dr. Kenneth M. Crowe for his collaboration in the early stages of the experiment and to Mr. Jack Garrison for the use of his liquid hydrogen target.

Mr. Robert Donaldson and Mr. Brook Knowles were of invaluable assistance throughout the experiment. Credit for the design of much of the electronic equipment is due Mr. Vern Ogren who, on many occasions, gave freely of his personal time to help with the experiment.

To the cyclotron crew, and especially to Mr. James Vale, I extend my sincere thanks for their cooperation during the bombardments.

This work was performed under the auspices of the AEC.

BIBLIOGRAPHY

1. W. F. Cartwright, C. Richman, M. N. Whitehead and H. A. Wilcox, Phys. Rev. 78, 823 (1950).
2. V. Z. Peterson, Phys. Rev. 79, 407 (1950); V. Z. Peterson, E. Iloff and D. Sherman, Phys. Rev. 81, 647 (1951).
3. K. Brueckner, Phys. Rev. 82, 598 Appendix (1951).
4. F. S. Crawford, K. M. Crowe, M. L. Stevenson, Phys. Rev. 82, 97 (1951).
5. F. S. Crawford, UCRL-2187 (Thesis).
6. J. Fischer, and J. Marshall, Rev. Sci. Inst. 23, 417 (1952).
7. R. Mather and E. Segré, Phys. Rev. 84, 191 (1951).
8. W. A. Aron, B. G. Hoffman and F. C. Williams, AECU-663 (second revision, 1949).
9. D. Stork, private communication.
10. A. Bloom, UCRL-1442
11. W. F. Cartwright, C. Richman, M. N. Whitehead and H. A. Wilcox, UCRL-2102.
12. V. Z. Peterson, E. Iloff, D. Sherman, Phys. Rev. 84, 372 (1951).
13. A. Schulz, D. Hamlin, M. Jakobson, and J. Merritt, Phys. Rev. 87, 219 (1952) and UCRL-1756.
14. R. Durbin, H. Loar, J. Steinberger, Phys. Rev. 84, 581 (1951).
15. D. Clark, A. Roberts and R. Wilson, Phys. Rev. 83, 649 (1951) and Phys. Rev. 85, 523 (1952).
16. R. Hildebrand, Phys. Rev. 89, 1090 (1953).
17. C. N. Yang, unpublished communication to C. Richman.
18. K. Watson and K. Brueckner, Phys. Rev. 83, 1 (1951).
19. A. Messiah, Phys. Rev. 86, 430 (1952).
20. K. Brueckner, R. Serber, and K. Watson, Phys. Rev. 81, 575 (1951).
21. W. Panofsky, R. L. Aamodt, and J. Hadley, Phys. Rev. 81, 565 (1951).
22. S. Tamor, Phys. Rev. 82, 38 (1951).
23. K. Brueckner and K. Watson, Phys. Rev. 86, 923 (1951).
24. K. Watson and C. Richman, Phys. Rev. 83, 1256 (1951).
25. G. Chew, M. Goldberger, J. Steinberger and C. Yang, Phys. Rev. 84, 581 (1951).
26. W. Rarita and J. Schwinger, Phys. Rev. 59, 436 (1941).

27. R. Marshak, Meson Physics, McGraw Hill, pg. 70.

28. R. Pease and H. Feshbach, Phys. Rev. 81, 142 (1951).

29. Proceedings of the Third Annual Rochester Conference on High Energy Physics, December 18-20, 1952.

30. M. Lévy, Phys. Rev. 86, 806 (1952); Phys. Rev. 88, 725 (1952) and A. Martin and L. Verlet, Phys. Rev. 89, 519 (1953).

31. R. Marshak and L. Foldy, Phys. Rev. 75, 1493 (1949).

32. K. Brueckner, Phys. Rev. 86, 106 (1952).

33. K. Crowe, UCRL-2050

34. W. Crandall, private communication.

FIGURE CAPTIONS

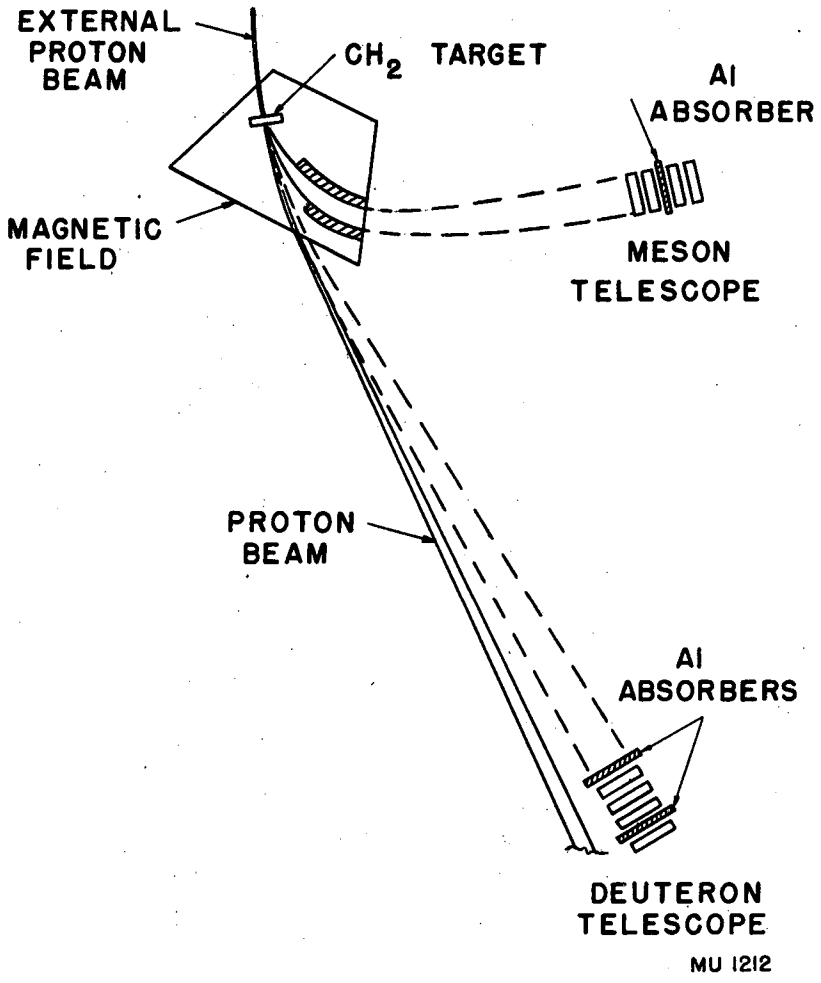

Fig. 1 Geometry of Preliminary Experiment

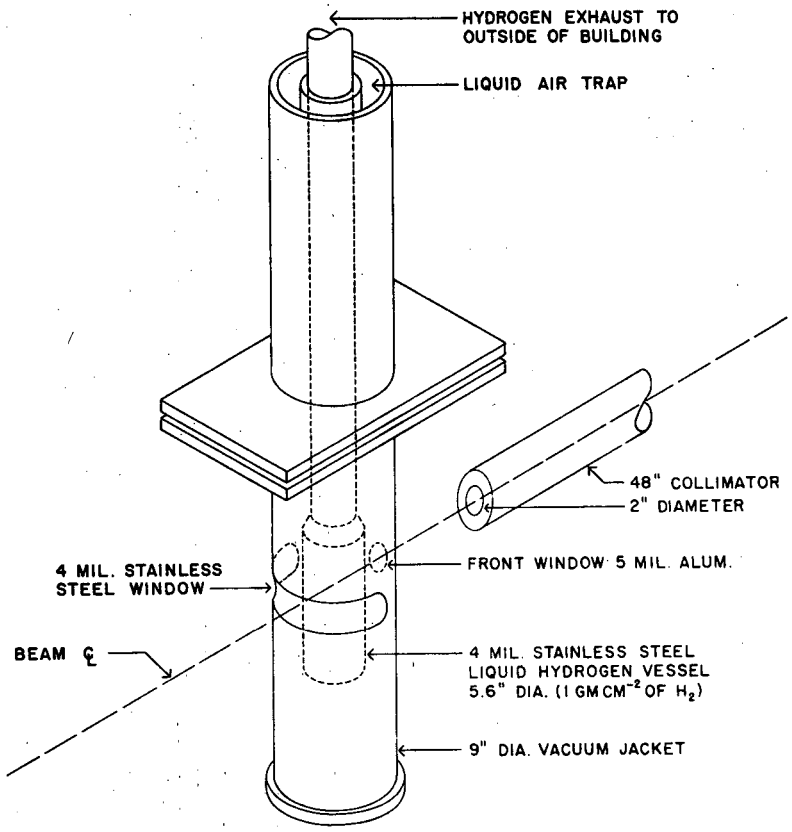

LIQUID HYDROGEN TARGET

MU-5314

Fig. 2a

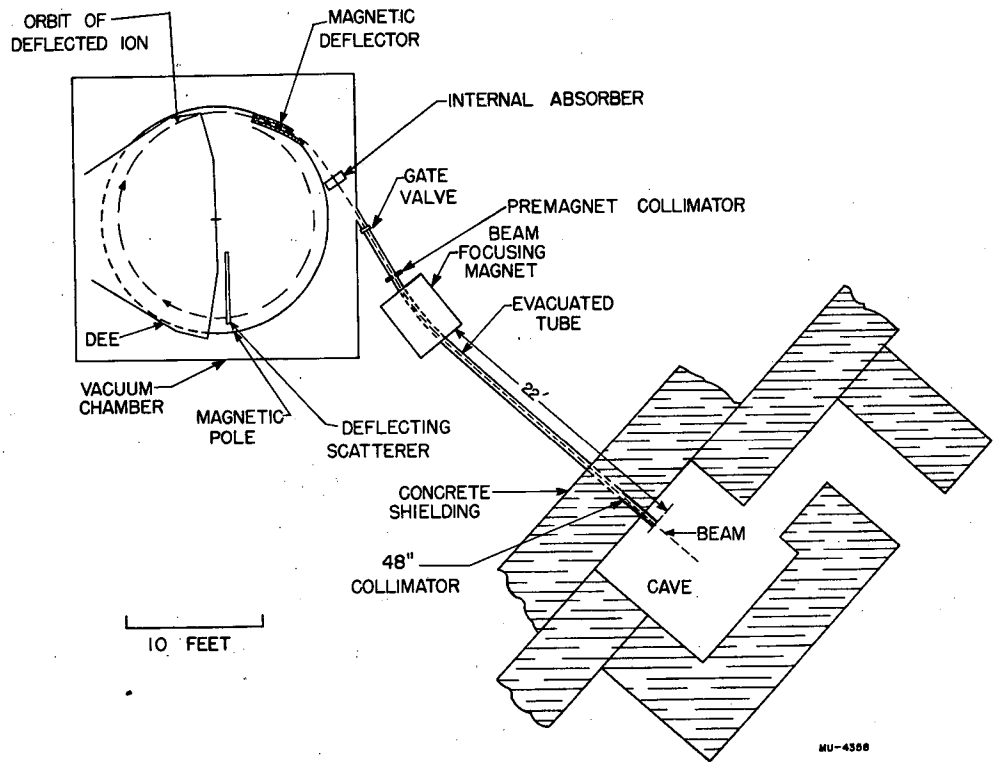

Fig. 2b Plan View of Cyclotron and External Beam

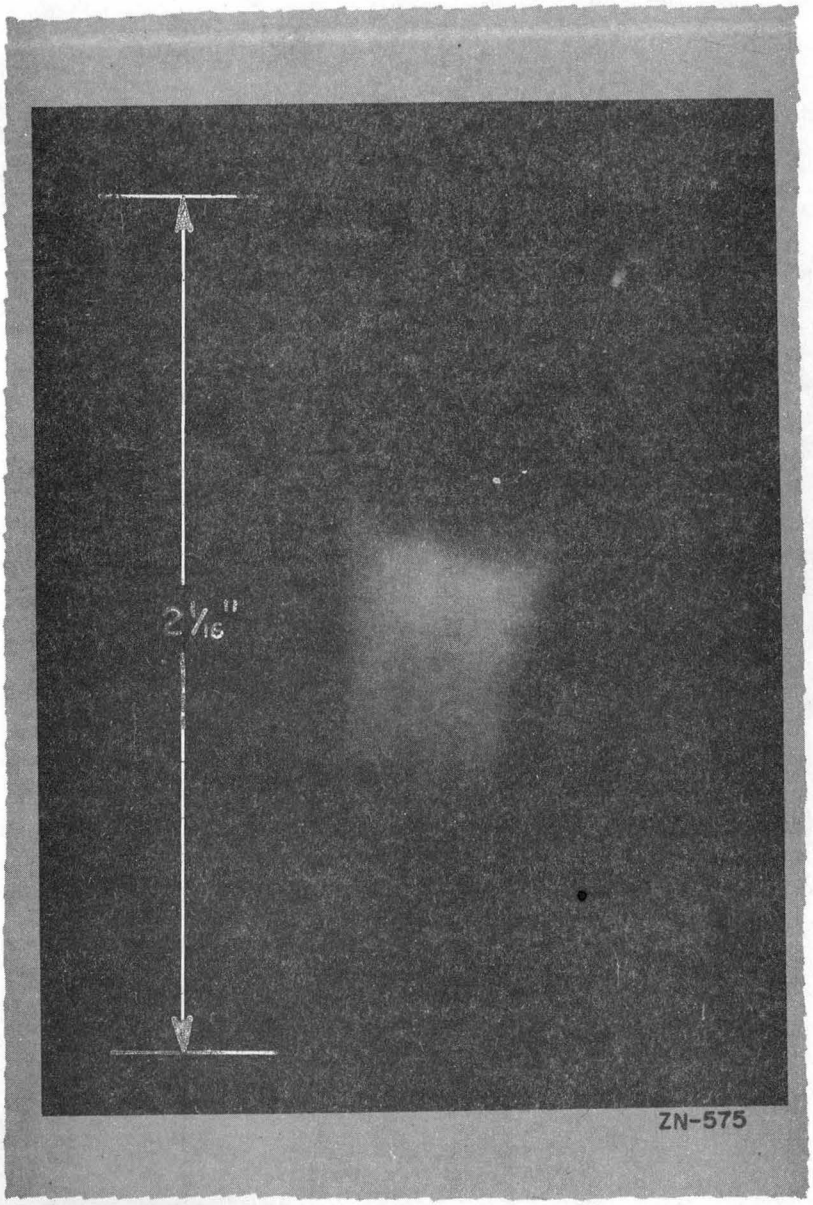

Fig. 3 Beam Configuration at the Target

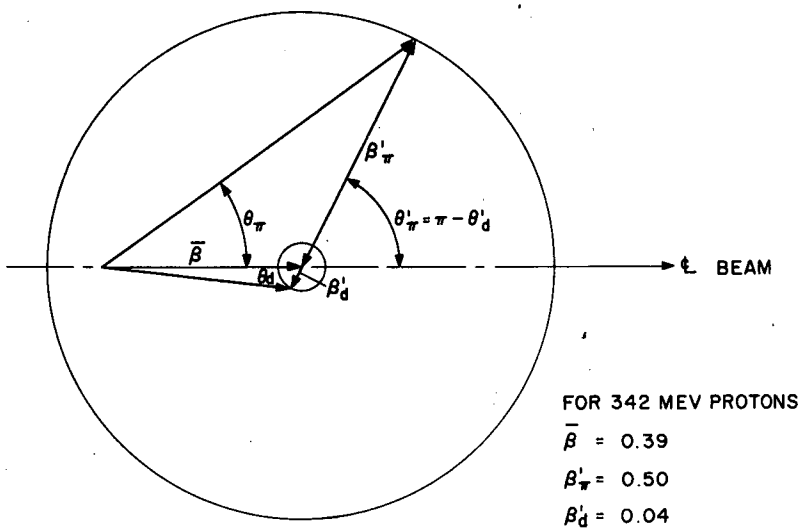

FOR 342 MEV PROTONS

$\bar{\beta}$ = 0.39

β'_π = 0.50

β'_d = 0.04

$\bar{\beta}$ = VELOCITY OF THE C.M. SYSTEM

β'_π = VELOCITY OF THE MESON IN THE C.M. SYSTEM

β'_d = VELOCITY OF THE DEUTERON IN THE C.M. SYSTEM

θ'_π = ANGLE OF THE MESON IN THE C.M. SYSTEM

θ_π = ANGLE OF THE MESON IN THE LABORATORY SYSTEM

θ_d = ANGLE OF THE DEUTERON IN THE LABORATORY SYSTEM

VELOCITY VECTOR DIAGRAM

MU-5210

Fig. 4

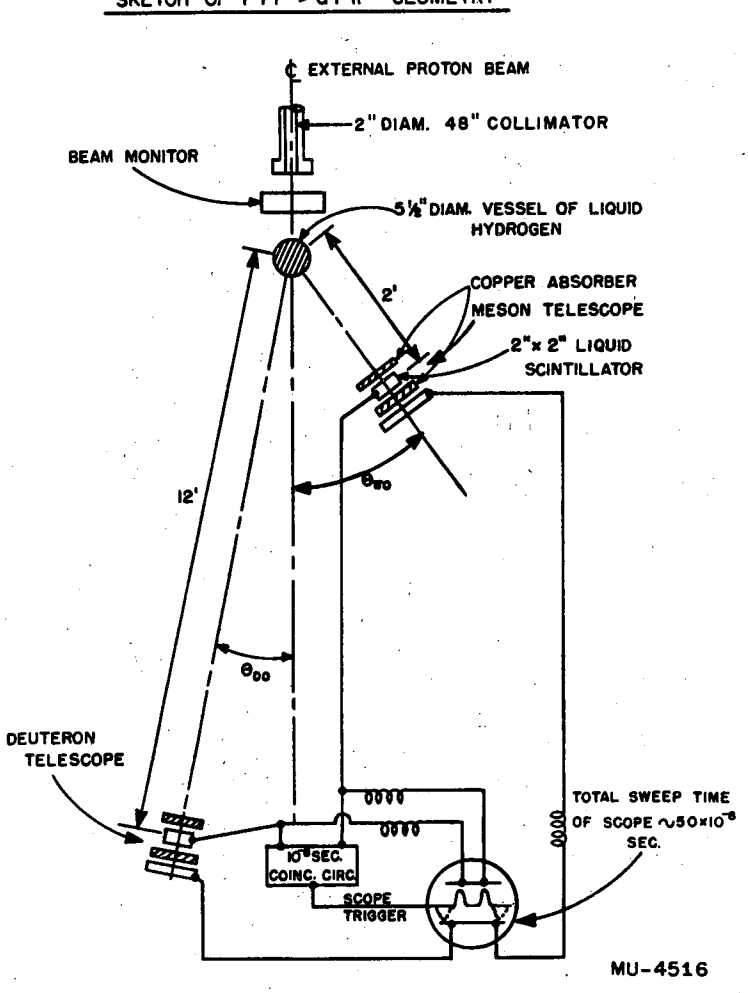
SKETCH OF P+P→d+π⁺ GEOMETRY
℄ EXTERNAL PROTON BEAM
2" DIAM. 48" COLLIMATOR
BEAM MONITOR
5½" DIAM. VESSEL OF LIQUID HYDROGEN
2'
COPPER ABSORBER
MESON TELESCOPE
2"x 2" LIQUID SCINTILLATOR
12'
θ₀₀
θ₀₀
DEUTERON TELESCOPE
TOTAL SWEEP TIME OF SCOPE ~50x10⁻⁸ SEC.
10⁻⁸ SEC. COINC. CIRC.
SCOPE TRIGGER
MU-4516

Fig. 5

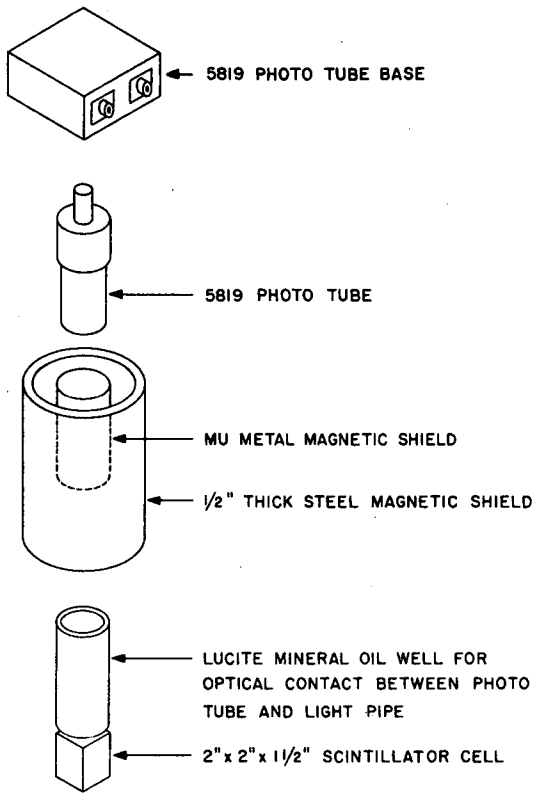

FIRST MESON COUNTER

MU-5312

Fig. 6

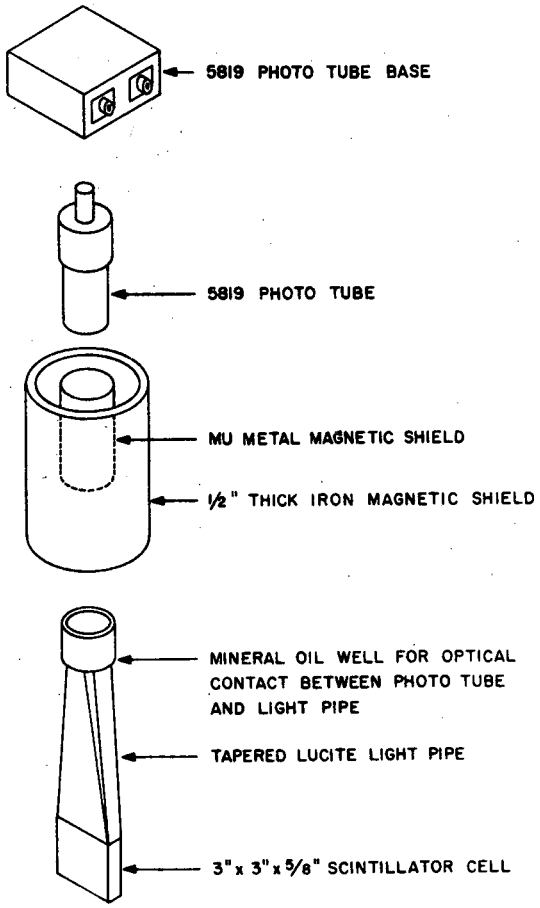
5819 PHOTO TUBE BASE
5819 PHOTO TUBE
MU METAL MAGNETIC SHIELD
½" THICK IRON MAGNETIC SHIELD
MINERAL OIL WELL FOR OPTICAL CONTACT BETWEEN PHOTO TUBE AND LIGHT PIPE
TAPERED LUCITE LIGHT PIPE
3" x 3" x 5/8" SCINTILLATOR CELL
FIRST DEUTERON COUNTER
MU-5313

Fig. 7

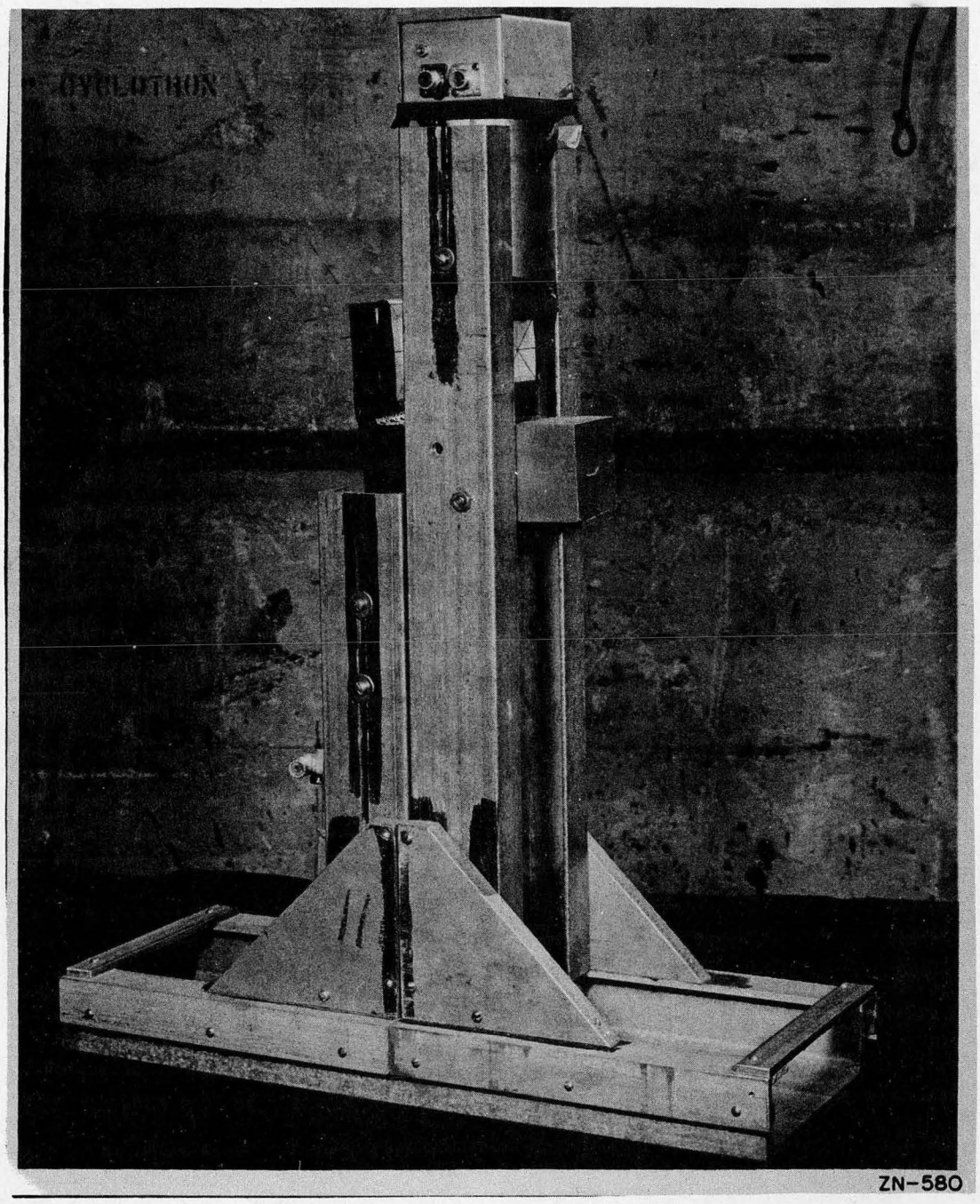

Fig. 8a Meson Telescope Assembly

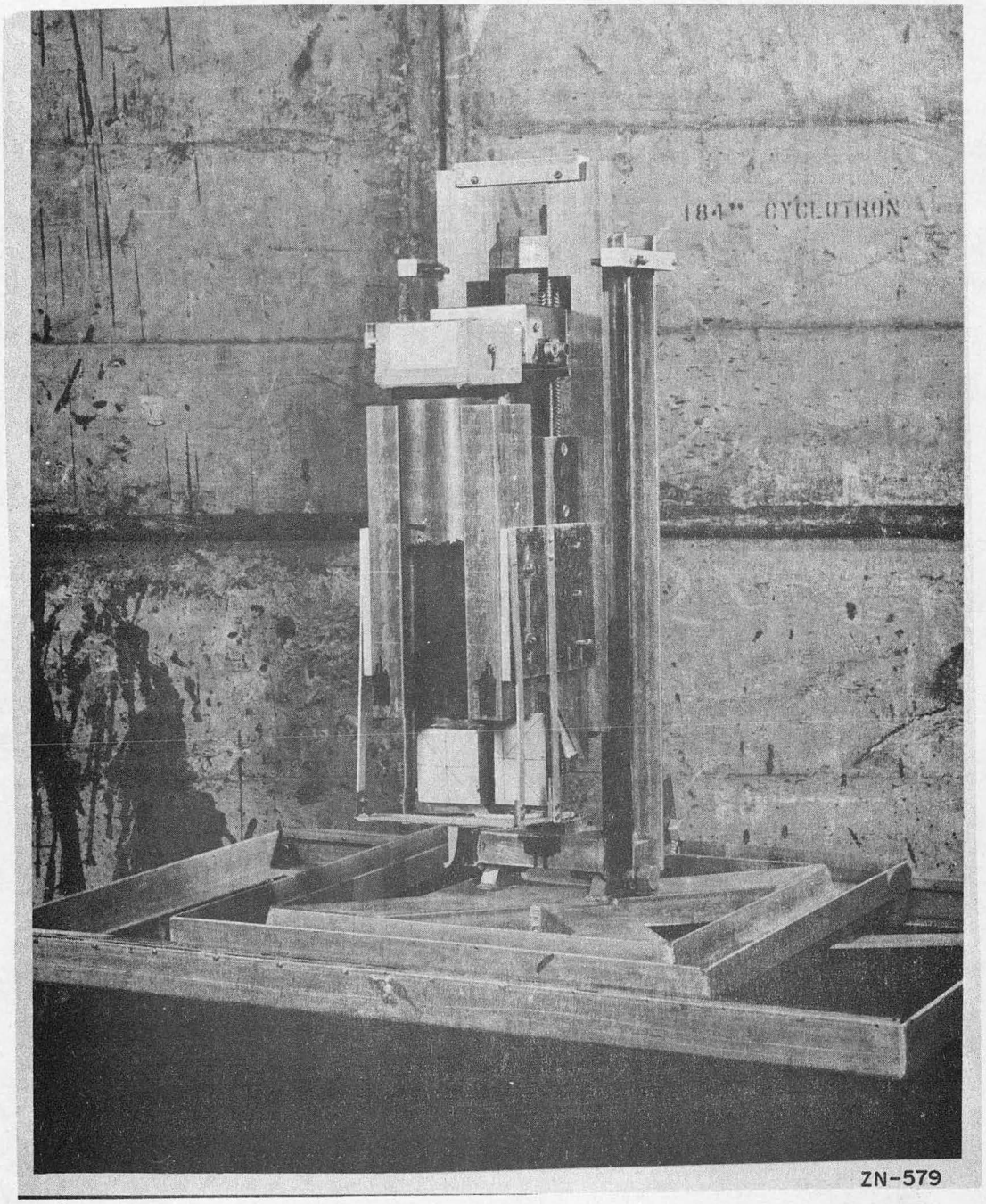

Fig. 8b Deuteron Telescope Assembly

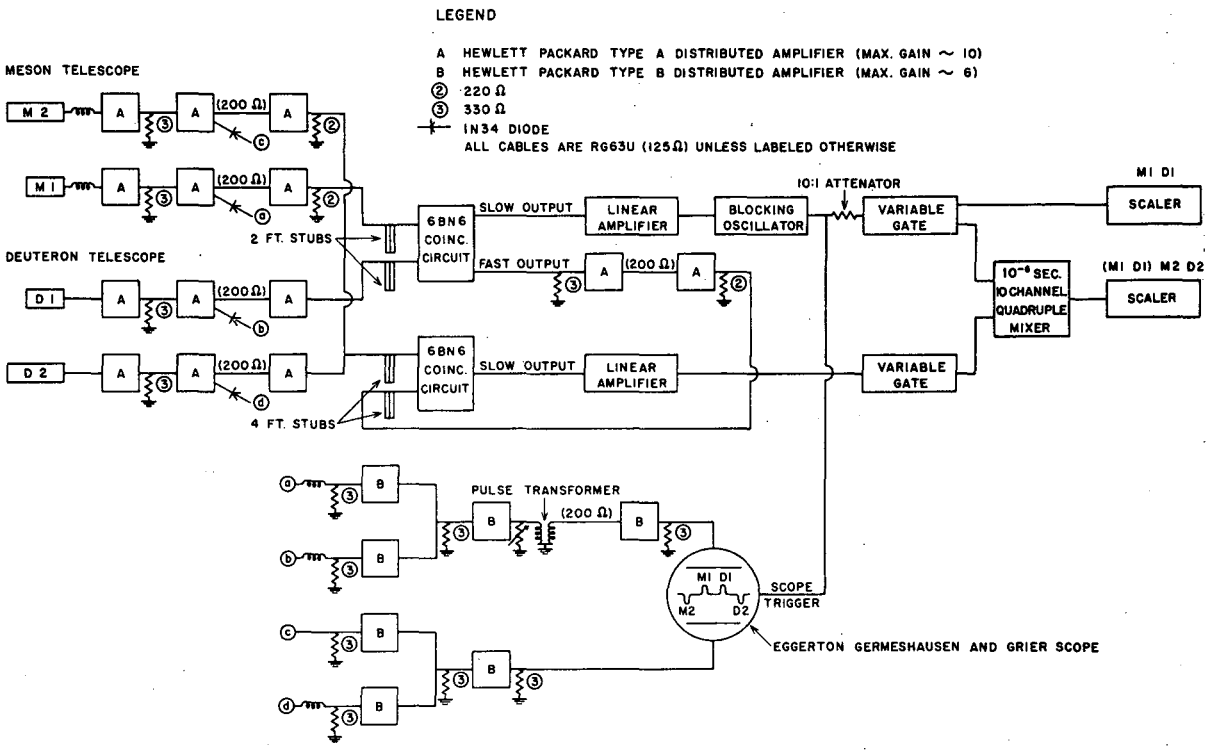

Fig. 9 Detailed Sketch of Electronics

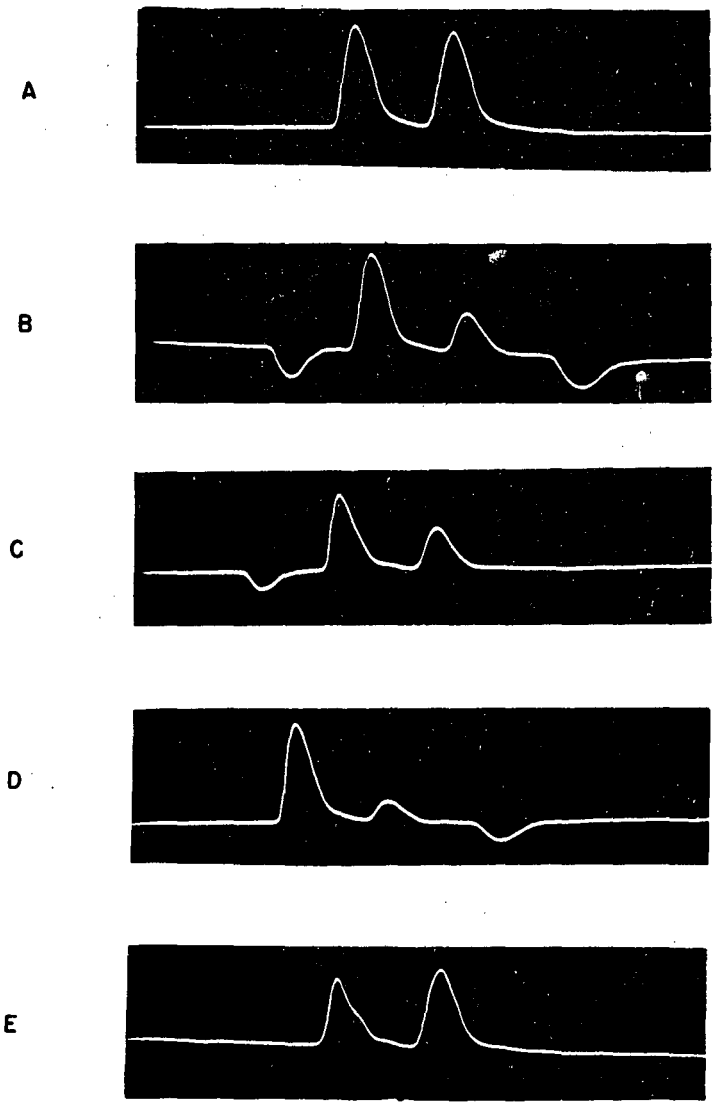

Fig. 10 Typical Oscilloscope Photographs

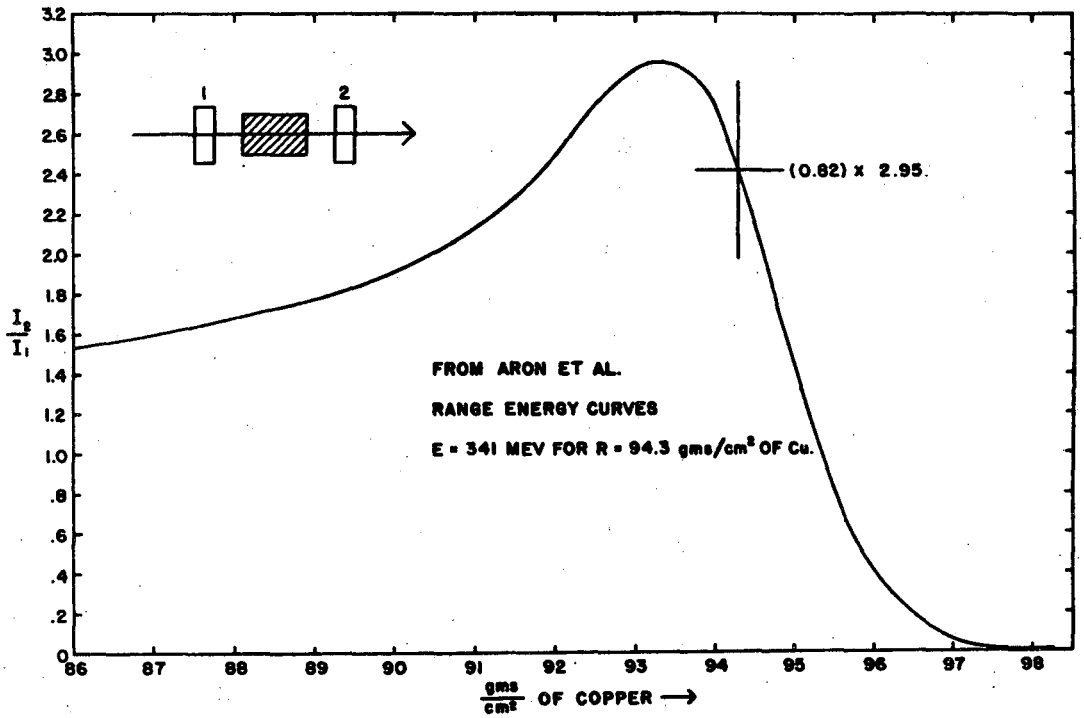

BRAGG CURVE FOR 341 MEV PROTONS

Fig. 11

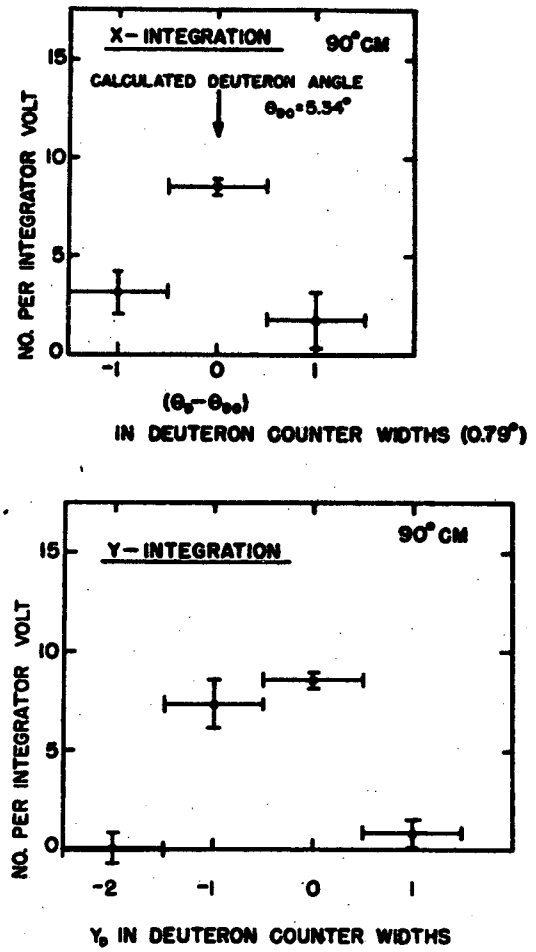

Fig. 12 Deuteron Integration Curves

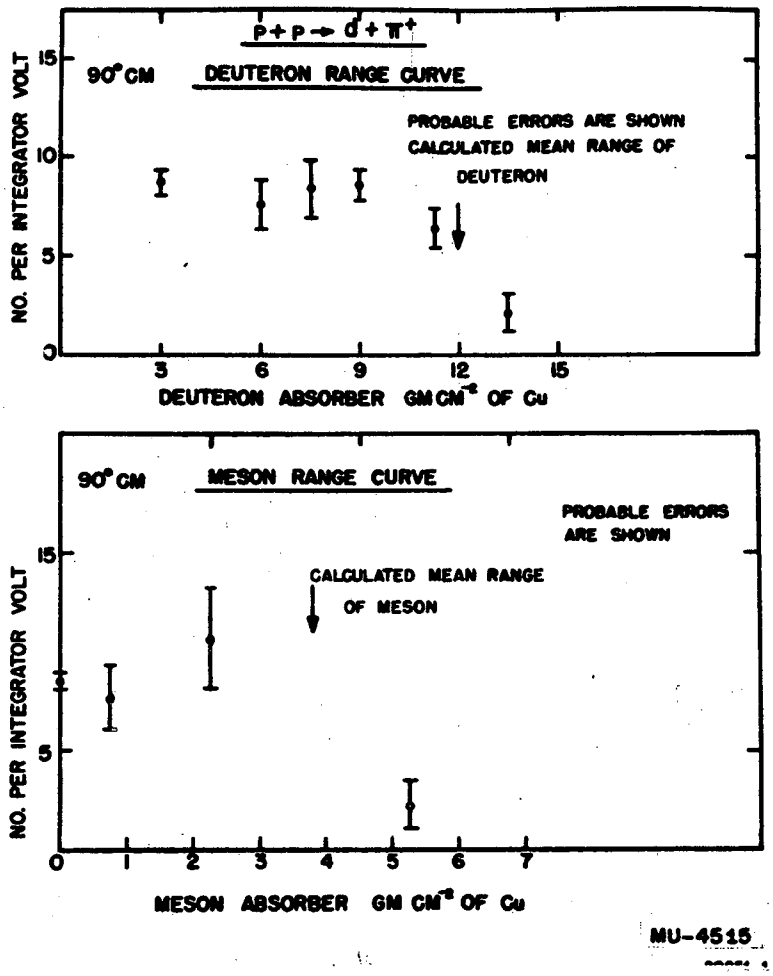

Fig. 13 Meson and Deuteron Range Curves

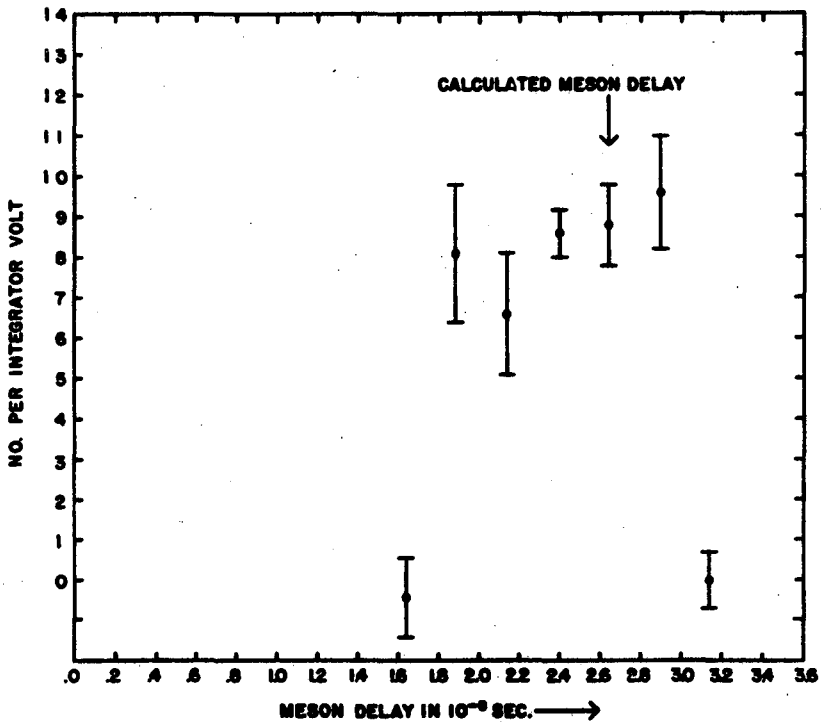
CALCULATED MESON DELAY
NO. PER INTEGRATOR VOLT
0 1 2 3 4 5 6 7 8 9 10 11 12 13 14
.0 .2 .4 .6 .8 1.0 1.2 1.4 1.6 1.8 2.0 2.2 2.4 2.6 2.8 3.0 3.2 3.4 3.6
MESON DELAY IN 10^{-8} SEC.
90° C.M. DELAY CURVE
MU-5182

Fig. 14

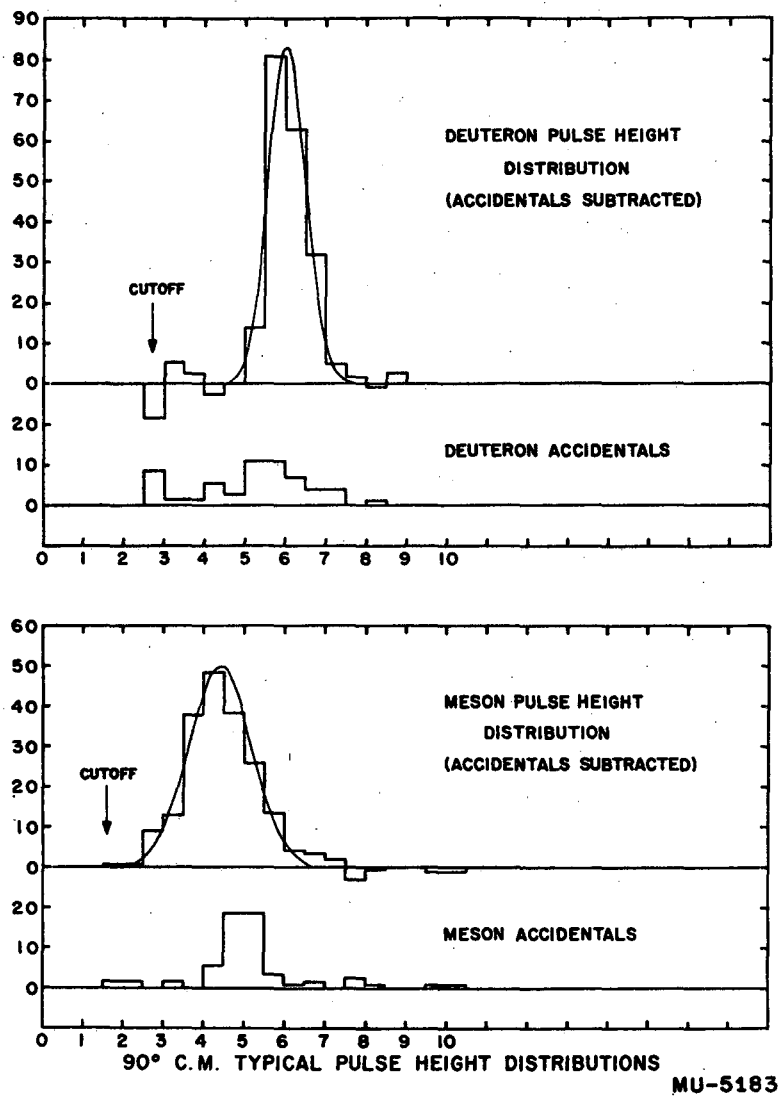
DEUTERON PULSE HEIGHT
DISTRIBUTION
(ACCIDENTALS SUBTRACTED)
CUTOFF
DEUTERON ACCIDENTALS
MESON PULSE HEIGHT
DISTRIBUTION
(ACCIDENTALS SUBTRACTED)
CUTOFF
MESON ACCIDENTALS
90° C.M. TYPICAL PULSE HEIGHT DISTRIBUTIONS
MU-5183

Fig. 15

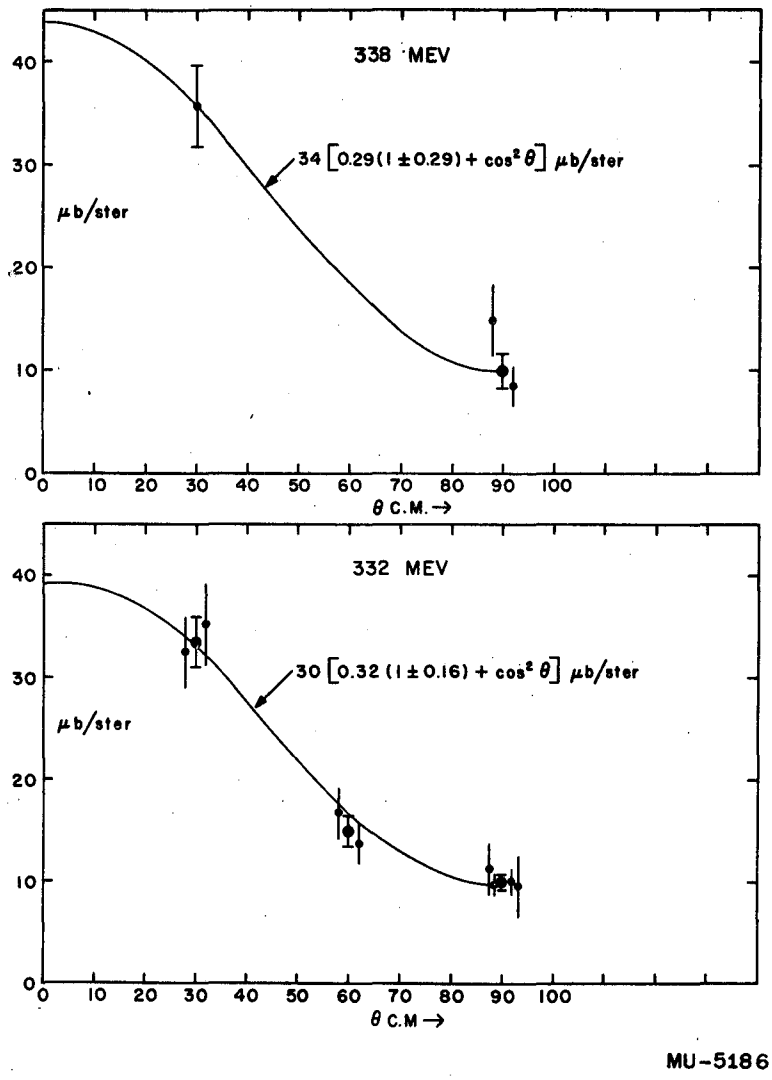

Fig. 16 Angular Distribution at 338 Mev, and 332 Mev.

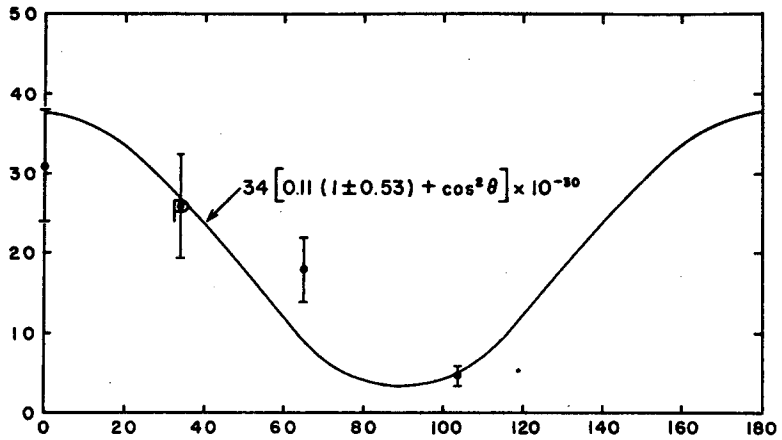

PROTON ENERGY = 341 $T_{\pi cm}$ = 22.5 MEV

$p+p\rightarrow\pi^{+}+d$ DATA OF CARTWRIGHT, RICHMAN, WHITEHEAD AND WILCOX PLUS V. PETERSON[12] ($\bar{P}$)

MU-5211

Fig. 17

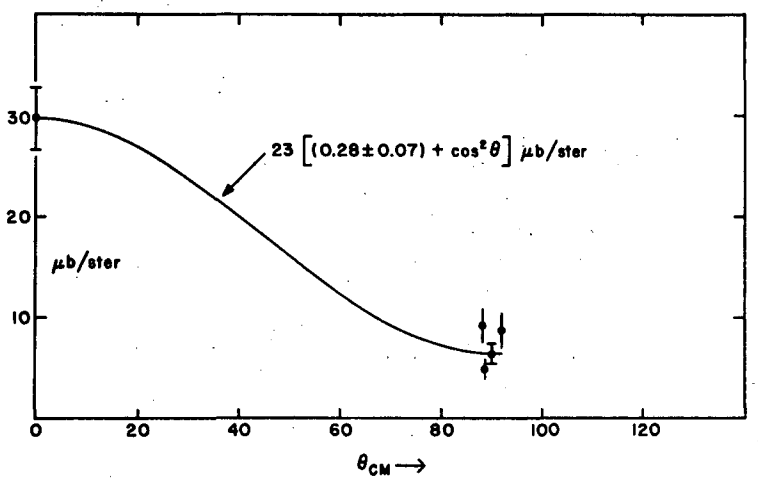

p + p ⟶ π⁺ + d DATA OF CRAWFORD AT 324 MEV

MU-5311

Fig. 18

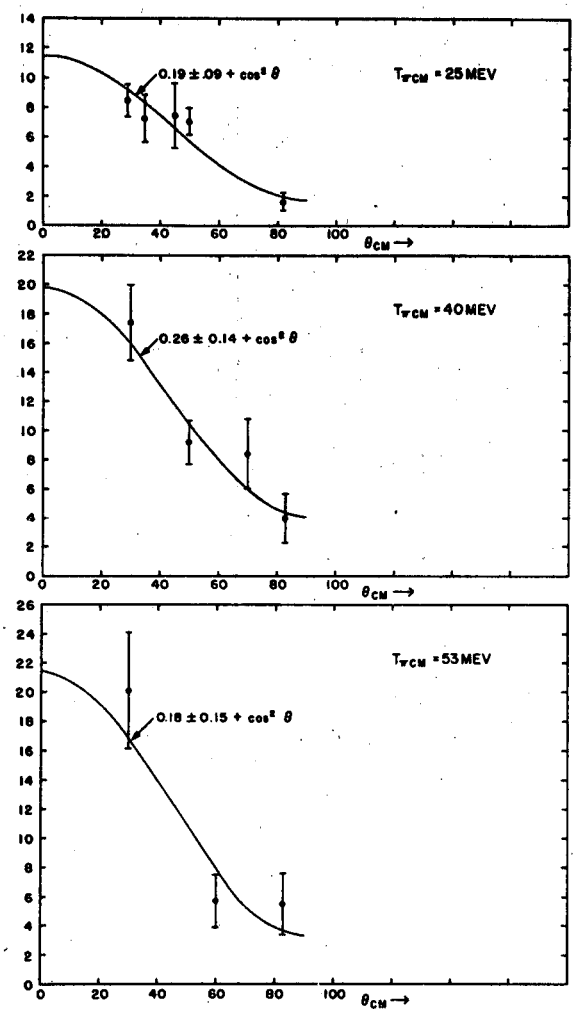

$\Pi^+ + d \longrightarrow p + p$ DATA OF DURBIN LOAR & STEINBERGER

MU-5208

Fig. 19

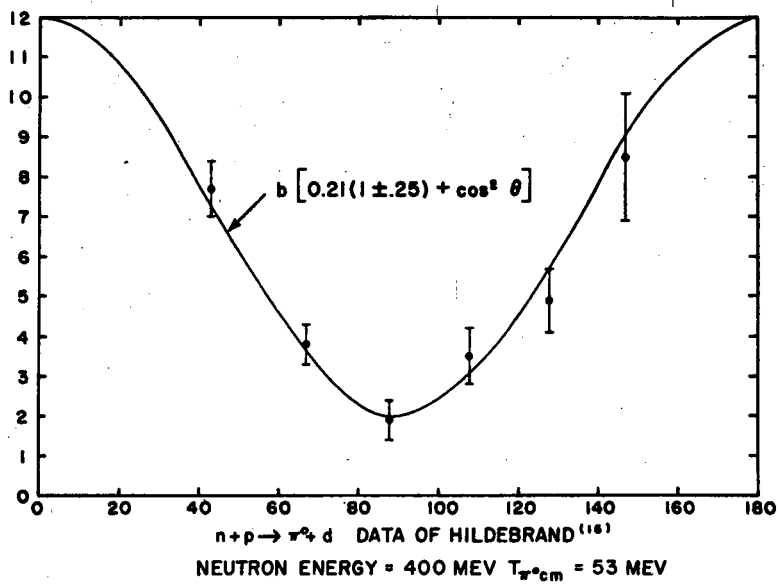

MU-5212

Fig. 20

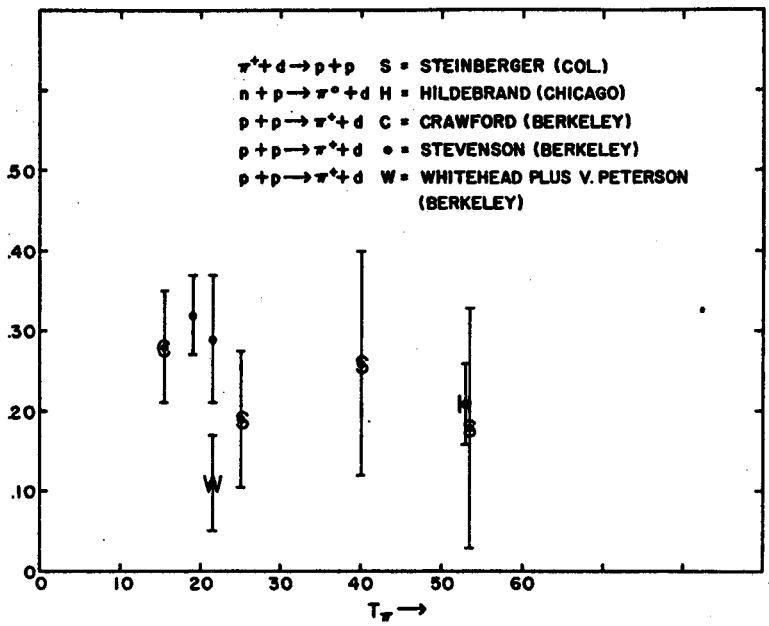

VARIATION OF "a" WITH ENERGY WHERE $\frac{d\sigma}{d\Omega} = b\,("a" + \cos^2\theta)$

MU-5185

Fig. 21